ISPRS Journal of Photogrammetry and Remote Sensing 181 (2021) 67–83

Contents lists available at ScienceDirect

ISPRS Journal of Photogrammetry and Remote Sensing

journal homepage: www.elsevier.com/locate/isprsjprs

Simultaneous investigation of surface and canopy urban heat islands over global cities

Huilin Du [a], Wenfeng Zhan [a,b,*], Zihan Liu [a], Jiufeng Li [a], Long Li [a], Jiameng Lai [a], Shiqi Miao [a], Fan Huang [a], Chenguang Wang [a], Chunli Wang [a], Huyan Fu [a], Lu Jiang [a], Falu Hong [a], Sida Jiang [a]

[a] Jiangsu Provincial Key Laboratory of Geographic Information Science and Technology, International Institute for Earth System Science, Nanjing University, Nanjing, Jiangsu 210023, China

[b] Jiangsu Center for Collaborative Innovation in Geographical Information Resource Development and Application, Nanjing 210023, China

ARTICLE INFO

Keywords:
Surface urban heat island
Canopy urban heat island
Thermal remote sensing
Surface properties
Population size
Climatic controls

ABSTRACT

Interpreting the similarities and dissimilarities in spatiotemporal variations and various controls between surface and canopy urban heat islands (UHIs) is critical for a better understanding of their vertical structure. Preceding comparisons of the surface UHI (SUHI) and canopy UHI (CUHI), however, remain mostly restricted either in a single city or over a few cities within limited background climates; therefore, the associated similarities and dissimilarities between the SUHI and CUHI under different climates, especially at a global scale, remain largely unknown. Based on both satellite and *in situ* data, we simultaneously investigated the spatiotemporal patterns of the SUHI intensity (SUHII) and CUHI intensity (SUHII) of 366 global cities within various background climates. We further investigated the different impacts of several controls (e.g., vegetation coverage, population size, precipitation) on SUHII and CUHII. Our results indicate the following: (1) For the selected 366 cities, the annual mean SUHII is higher than CUHII by 1.1 ± 1.9 °C (mean ± Std) during the day and 0.3 ± 1.5 °C (mean ± Std) at night. The SUHII and CUHII in the equatorial, warm temperate, and snow climates are generally consistent with the above characteristics (i.e., SUHII > CUHII), however, in arid regions SUHII is lower than CUHII by 0.8 °C during the day. (2) The annual mean day–night difference in SUHII is positive (i.e., 0.6 ± 1.8 °C (mean ± Std)), while the difference in CUHII becomes negative (i.e., −0.2 ± 1.6 °C (mean ± Std)), indicating that urbanization increases the diurnal temperature range (DTR) based on land surface temperature, but it decreases the DTR based on surface air temperature. (3) Despite the high correlation between vegetation coverage and impervious surface percentage (ISP), their impacts on SUHII and CUHII were not consistent. The urban–rural difference in ISP exerts an insignificant impact on both SUHII and CUHII during the day and a greater impact on CUHII than on SUHII at night, whereas the urban–rural difference in vegetation coverage has a greater impact on SUHII than on CUHII during the day, while the opposite occurs at night. The impacts of population size on SUHII and CUHII are much greater during the night than on the day in which their impacts can be minimal. The relationship between annual mean precipitation and SUHII is positive during the day but negative at night, while for CUHII, their relationship is insignificantly negative both during the day and at night. These results can improve our understanding of the spatiotemporal patterns and controls of these two types of UHIs under various climates.

1. Introduction

In recent years, rapid urbanization has led to drastic changes in the urban environment (Wohlfahrt et al., 2019). One of the changes is the urban heat island (UHI) effect, a phenomenon with warmer temperatures in urban surfaces than in rural surroundings (Aida and Yaji, 1979; Jin, 2012; Oke, 1982). Understanding and monitoring UHIs have become a focus of urban climate research (Li et al., 2021; Oleson et al., 2015; Paschalis et al., 2021; Stewart, 2019), mostly because of its serious negative impacts on the urban environment (Santamouris, 2020) and human health (Tan et al., 2010). Previous studies have investigated both the surface UHI (SUHI) and canopy UHI (CUHI) based on satellite-derived land surface temperature (T_s) and site-based air temperature (T_a), respectively. The physical representations of T_s and T_a are closely related, yet they also differ in many aspects (Good, 2016; Jin and Dickinson, 2010). T_s can be easily obtainable regularly and directly with satellite thermal sensors over a large scale (Huang and Wang, 2019;

* Corresponding author at: Nanjing University at Xianlin Campus, No. 163 Xianlin Avenue, Qixia District, Nanjing, Jiangsu 210023, China.
E-mail address: zhanwenfeng@nju.edu.cn (W. Zhan).

https://doi.org/10.1016/j.isprsjprs.2021.09.003
Received 2 April 2021; Received in revised form 31 August 2021; Accepted 3 September 2021
Available online 16 September 2021

Nomenclature

Abbreviations and symbols

CUCI	canopy urban cool island
CUHI	canopy urban heat island
CUHII	CUHI intensity
$CUHII_{day}$	daytime CUHII
$CUHII_{ngt}$	nighttime CUHII
DTR	diurnal temperature range
ISA	impervious surface area
ISP	impervious surface percentage
PREP	precipitation
SUCI	surface urban cool island
SUHI	surface urban heat island
SUHII	SUHI intensity
$SUHII_{day}$	daytime SUHII
$SUHII_{ngt}$	nighttime SUHII
$SUHII_{pixel}$	SUHII based only on the land surface temperature of the pixels where the station pairs are located
$SUHII_{pixel\_day}$	daytime $SUHII_{pixel}$
$SUHII_{pixel\_ngt}$	nighttime $SUHII_{pixel}$
UHI	urban heat island
UHII	UHI intensity
$UHII_{day}$	daytime UHII
UHI_{ngt}	nighttime UHII
ΔCUHII	day–night difference of CUHII
ΔDist%	ratio of distance between the urban and rural stations to the urban center
ΔDTR	urbanization-induced variations in DTR
ΔEVI	urban–rural difference in vegetation coverage
ΔISP	urban–rural difference in impervious surface percentage
ΔSUHII	day–night difference of SUHII
ΔWSA	urban–rural difference in albedo
log(*P*)	logarithm of urban population
T_a	surface air temperature
T_{max}	maximum T_a
T_{min}	minimum T_a
T_s	land surface temperature
δ	standard deviation
δh_1	daytime time difference between T_s and T_a
δh_2	nighttime time difference between T_s and T_a
δh_3	time difference in daily maximum T_a between urban and rural areas
δh_4	time difference in daily minimum T_a between urban and rural areas

Weng, 2009), but it can often be invalidated by cloud contamination (Sun et al., 2017) and is highly sensitive to surface properties (Li et al., 2013). In comparison, T_a appears to be more homogeneous due to near-surface atmospheric turbulence and mixing (Good, 2016). T_a is often obtained by ground-based stations with a high observation frequency and accuracy, but is usually affected by the sparse and uneven distribution of stations (Sheng et al., 2017). A combination of T_s and T_a to investigate the SUHI and CUHI simultaneously provides more comprehensive knowledge of the spatiotemporal characteristics of UHIs (Jin, 2012; Li and Zha, 2019; Yang et al., 2020).

The SUHI and CUHI have been examined simultaneously on local (Anniballe et al., 2014; Bonafoni et al., 2015; Chakraborty et al., 2017; Cui and De Foy, 2012; Ho et al., 2016; Hu et al., 2019; Huang et al., 2020; Li et al., 2017; Schwarz et al., 2012; Sheng et al., 2017; Wang et al., 2020; Yang et al., 2020; Zhang et al., 2014a) or regional scales (Li and Zha, 2019; Sun et al., 2020; Venter et al., 2021; Zhang et al., 2014b). These studies have indicated that there are differences in the patterns of the diurnal and seasonal variations between the SUHI and CUHI, and the differences are not consistent among cities under different background climates.

In terms of diurnal variations, the SUHI intensity (SUHII) is usually greater than the CUHI intensity (CUHII), and the difference between these two intensities is greater during the day than at night (Anniballe et al., 2014; Chakraborty et al., 2017; Sun et al., 2015; Venter et al., 2021; Zhang et al., 2014b). For example, during the summer daytime, SUHII was stronger than CUHII by 9.4 °C in Milan (Anniballe et al., 2014), and by approximately 2.0 °C for European 342 urban clusters (Venter et al., 2021), and the difference between SUHII and CUHII, in Beijing, is more than 2.0 °C during the day in all seasons, with a larger difference in summer than in winter (Sun et al., 2015). In contrast, the difference between SUHII and CUHII was generally smaller at night. At night, the SUHII only slightly surpasses CUHII (less than 2.0 °C) in Milan (Anniballe et al., 2014), Beijing (Sun et al., 2015), Leipzig (Schwarz et al., 2012) and European 342 urban clusters (Venter et al., 2021).

In terms of seasonal variations, during the daytime, SUHII is relatively less affected by background climate than CUHII (Hu et al., 2019). Specifically, daytime SUHII is usually stronger in the summer (Li et al., 2017; Sheng et al., 2017; Wang et al., 2017; Yang et al., 2020). For daytime CUHII, although Beijing and Changchun are both located in the temperate monsoon climate zone, the former has a stronger daytime CUHII in summer than in winter (Wang et al., 2017), while the latter exhibits the converse trend (Yang et al., 2020). The significant difference in seasonal variation of daytime CUHII is also manifested in Wuhan (Li et al., 2017) and Hangzhou (Sheng et al., 2017), both with a subtropical monsoon climate. At night, the seasonal variations of SUHII and CUHII both show significant differences depending on the background climate. For example, the nighttime SUHII reaches a maximum in summer in Birmingham, with a temperate maritime climate (Zhang et al., 2014a), while it becomes the strongest in winter in Beijing (Hu et al., 2019). The nighttime CUHII is greater in summer than in winter in Birmingham (Zhang et al., 2014a), but the opposite occurs in Hangzhou (Sheng et al., 2017).

Previous studies have also directly compared or indirectly indicated the discrepancies in various controls for these two types of UHIs (Anniballe et al., 2014; Chakraborty et al., 2020; Clinton and Gong, 2013; Hu et al., 2019; Imhoff et al., 2010; Lai et al., 2021; Li et al., 2019; Li et al., 2020a; Manoli et al., 2019; Manoli et al., 2020a; Miles and Esau, 2020; Oke, 1973; Paschalis et al., 2021; Peng et al., 2012; Sun et al., 2015; Venter et al., 2021; Wang et al., 2017; Zhao et al., 2014). These controls can be divided into three main categories: surface properties (i.e., albedo, vegetation coverage, impervious surface percentage), overall urbanization metric (i.e., urban area, urban population, urban size), and climatic controls (i.e., air temperature, precipitation).

The first is the investigation of surface properties on SUHI and/or CUHI (Anniballe et al., 2014; Li and Zha, 2019; Venter et al., 2021; Wang et al., 2017). Such studies have indicated that vegetation coverage has a greater influence on SUHII than CUHII at both day and night (Anniballe et al., 2014; Venter et al., 2021). The ISP exerts a larger impact on SUHII during the day but influences CUHII more at night (Venter et al., 2021; Wang et al., 2017). The urban–rural difference in albedo is positively correlated with SUHII during the day, but their correlation becomes the opposite at night (Li et al., 2020b; Peng et al., 2012); while this surface parameter is negatively correlated with the daily mean CUHII (Li and Zha, 2019). Besides, this urban–rural albedo difference influences SUHII more than CUHII at both day and night (Venter et al., 2021). The second is the examination of the overall urbanization metric on SUHI and CUHI. For example, previous studies have indicated that the logarithm of urban size (or urban population)

has a linearly positive relationship with both SUHII (Clinton and Gong, 2013; Miles and Esau, 2020; Zhao et al., 2014) and CUHII (Oke, 1973). The last is the investigation of climatic controls on these two types of UHIs (He, 2018; Hu et al., 2019; Lai et al., 2021; Li et al., 2019; Li et al., 2020a; Manoli et al., 2019; Peng et al., 2012; Wang et al., 2020; Zhao et al., 2014). These studies have revealed that the correlation between the annual mean precipitation (PREP) and SUHII is usually positive during the day but negative at night (Lai et al., 2021; Li et al., 2019; Li et al., 2020a; Peng et al., 2012; Zhao et al., 2014), whereas the annual mean PREP often poses a negative impact on the daily mean CUHII (Hu et al., 2019).

Previous studies on the simultaneous investigation of SUHI and CUHI have been mostly limited in a single city or over a few cities. A few studies have examined these two types of UHIs concurrently over a large number of cities in United States (Zhang et al., 2014b) and in Europe (Venter et al., 2021), yet they have focused either on limited climates (e.g., warm temperate climate) or on specific time periods (e.g., heat wave period or summer and winter). Thus, despite great progress achieved by preceding studies, two issues remain to be addressed. First, the differences in the spatiotemporal variations between SUHII and CUHII for cities within abundant types of climates remain largely not clear. Second, the different impacts from various controls on these two types of UHIs have not been clarified uniformly and consistently for cities in a great variety of background climates over a large scale.

Facing these challenges, we investigated SUHII and CUHII across 366 global cities by combining both satellite and *in situ* data. The main objectives include: (1) investigating the spatiotemporal patterns of SUHII and CUHII for these 366 cities and (2) investigating the relationships between typical controls (i.e., surface properties, overall urbanization metric, climatic controls) and SUHII and CUHII. We believe that our research can assist an improved understanding of both surface and canopy UHIs.

2. Study area and data

2.1. Study area

In this study, a total of 366 global cities with urban areas exceeding 10 km^2 were selected, mostly considering whether there are usable urban–rural station pairs of *in situ* T_a measurements within a city (Fig. 1) (more details on city selection are given in Section 3.1.2). The resulting 366 cities are distributed in four climatic zones according to the Köppen–Geiger classification scheme (Kottek et al., 2006), including the equatorial (10 cities), arid (43 cities), warm temperate (203 cities), and snow zones (110 cities). These cities can also be divided into four groups depending on city size (OECD, 2021), including 234 small cities (with urban population < 0.2 million), 52 medium cities (0.2–0.5 million), 43 large cities (0.5–1.5 million), and 37 mega cities (>1.5 million). Note that the mid-latitude and high-latitude cities in warm temperate and snow climates were incorporated here, partly because the UHI effect may provide benefits to these cities by producing additional heat that could be helpful for urban residents (Martilli et al., 2020a; Oke et al., 2017; Sun and Augenbroe, 2014; Yang and Bou-Zeid, 2018), and partly because it has been very common to investigate the UHIs of these cities in previous studies that concentrating on a very large scale (Chakraborty and Lee, 2019; Clinton and Gong, 2013; Imhoff et al., 2010; Peng et al., 2012; Varquez and Kanda, 2018).

2.2. Data

The data used in this stuy included meteorological measurements, MODIS images, reanalysis data and auxiliary data. The meteorological data were used primarily to calculate CUHII and for the associated sensitivity analysis. The MODIS data were applied mainly to calculate SUHII and investigate the impacts of the vegetation index and surface albedo on SUHII and CUHII. The reanalysis data were utilized to explore the impacts from climatic controls (i.e., air temperature, precipitation) on SUHII and CUHII, and the auxiliary data were employed primarily to determine the urban boundary and analyze the impacts of population and ISP on SUHII and CUHII.

2.2.1. Meteorological data

We employed T_a measurements in 2012 from two sources, i.e., the Breakpoint Adjusted Monthly Station dataset downloaded from Berkeley Earth (http://berkeleyearth.org/) and the China Meteorological Science Data Center (CMSDC, http://data.cma.cn/). This dataset provides a collection of adjusted and homogeneous monthly mean maximum and minimum T_a data collected over more than 20,000 ground-based stations globally (Rohde et al., 2013). Considering that the station number within this dataset is relatively limited across China, we further incorporated more monthly mean T_a data from the CMSDC, which consists of T_a data at over 2,400 stations. The T_a datasets from these two sources were used for the selection of urban–rural station pairs and the calculation of CUHII (refer to Sections 3.1, 3.2). We further employed hourly

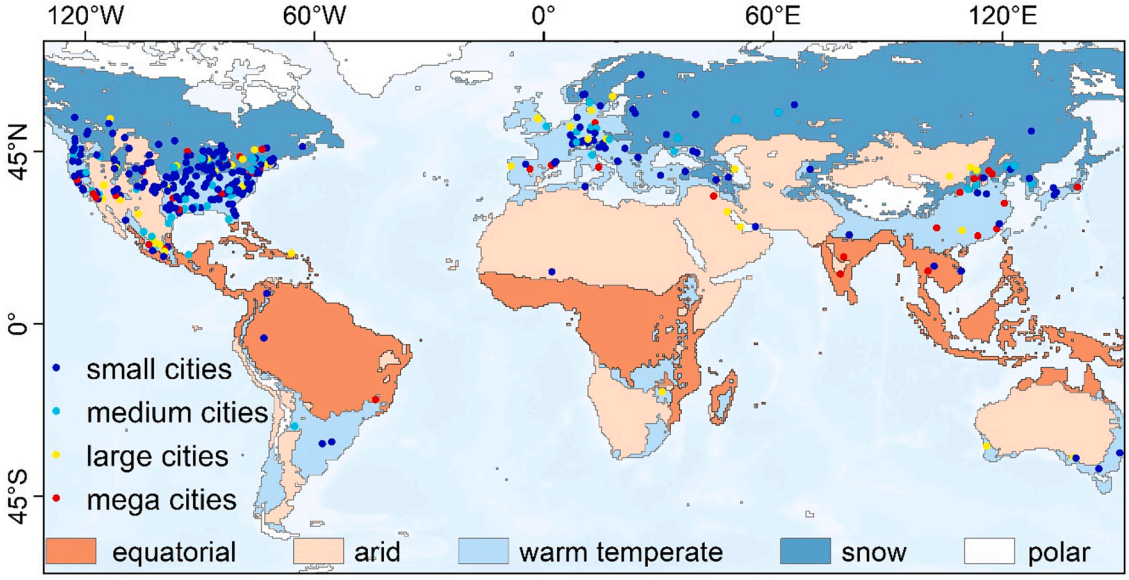

Fig. 1. Distribution of the selected 366 cities worldwide.

T_a measurements densely distributed in three cities, including Beijing (316 sites), Shenyang (246 sites), and Guangzhou (339 sites), also obtained from the CMSDC. This hourly dataset was applied to test the impacts from the representativeness of the chosen urban–rural station pairs as well as from the data acquisition time differences between *in situ* T_a and satellite-derived T_s (refer to Section 5.2).

2.2.2. MODIS data

The daily T_s product (MYD11A1, with a spatial resolution of 1 km), 16-day composite EVI product (MYD13A2, 1 km), 16-day composite albedo product (MCD43B3, 1 km), and yearly land cover type product (MCD12Q1, 0.5 km) in 2012 were employed in this study (Table 1). The T_s and land-cover type data were used for calculating SUHII. The retrieval errors of the T_s data are within ± 1.0 °C in most cases (Wan and Dozier, 1996). Here, we only employed the T_s data from Aqua/MODIS rather than from Terra/MODIS because the transit times of the former satellite (i.e., 13:30 and 01:30 local solar time) are relatively closer to the times of daily maximum and minimum T_a (Oke et al., 2017). A total of 17 land cover types defined by the International Geosphere-Biosphere Program classification scheme were used to eliminate the pixels labeled as water, snow and ice, and permanent wetlands (Lai et al., 2018). The EVI and white sky albedo (WSA) data were used to investigate the impacts of the urban–rural difference in vegetation abundance and surface albedo on SUHII and CUHII.

2.2.3. Reanalysis data

The reanalysis data in 2012 provided by the TerraClimate dataset (http://www.climatologylab.org/terraclimate.html), including the monthly maximum and minimum air temperature and precipitation, were employed to investigate the impacts from climatic controls on SUHII and CUHII. This is a dataset that includes most monthly climatic variables for global terrestrial surfaces with a spatial resolution of 2.5 arc minutes (approximately 4 km), and its overall accuracy is generally higher than other similar coarse-resolution gridded datasets (Abatzoglou et al., 2018).

2.2.4. Auxiliary data

The auxiliary data consist of urban boundary, elevation, impervious surface area, and population data (Table 1). Global urban boundary (GUB) data were derived from the global artificial impervious area (GAIA) product (Li et al., 2020c) and were used to determine urban areas. The digital elevation data obtained from GTOPO30 with a spatial resolution of 30 arc-seconds (approximately 900 m) were employed to eliminate pixels/stations with an elevation of ± 50 m from the median elevation of the urban pixels (Imhoff et al., 2010; Lai et al., 2018; Venter et al., 2021; Zhang et al., 2014b). Note that the median rather than the mean elevation was employed here to eliminate fragmentary urban pixels with extremely high or low elevations. The impervious surface area, with a spatial resolution of 30 m, was obtained from the global artificial impervious area (GAIA) product, which has a mean overall accuracy exceeding 90% (Gong et al., 2020). The GAIA product was used to identify appropriate urban–rural station pairs and analyze the impact from ISP on SUHII and CUHII. The population data were derived from GPWv411 with a spatial resolution of 30 arc seconds (Doxsey-Whitfield et al., 2015), and were employed to categorize cities according to city size as well as to investigate the impacts of population on SUHII and CUHII. The digital elevation and population data were resampled to 1 km using the nearest neighbor method to match the spatial resolution of the T_s data (Clinton and Gong, 2013; Lai et al., 2018).

Table 1
Detailed information on the satellite and auxiliary data.

Variable	Product	Temporal resolution	Spatial resolution	Data year
LST	MYD11A1	Daily	1 km	2012
EVI	MYD13A2	16-day	1 km	2012
Albedo	MCD43B3	16-day	1 km	2012
Land cover type	MCD12Q1	Yearly	500 m	2012
Population	GPWv411	Five years	30 arc s	2010
Elevation	GTOPO30	–	30 arc s	–
Impervious surface area	GAIA	Yearly	30 m	2012
Global urban boundary	GUB	Five years	–	2010

3. Methods

The differences between SUHII and CUHII in terms of spatiotemporal variations and various controls were investigated using the following three steps. (1) *Delineation of urban and rural areas and the selection of appropriate urban–rural station pairs*: The urban and rural areas were delineated based on urban boundaries, land use type, and DEM data (Section 3.1.1), and the appropriate urban–rural station pairs were identified by associating with the ISP information (Section 3.1.2). (2) *Calculation and simultaneous investigation of SUHII and CUHII*: The SUHII and CUHII of all cities were estimated (Section 3.2.1), and their differences in temporal (seasonal and diurnal) and spatial (various climate zones) variations were analyzed (Section 3.2.2). (3) *Investigation into controls of SUHII and CUHII*: The impacts from surface properties, overall urbanization metric, and climatic controls on SUHII and CUHII were examined across various climates and seasons (Section 3.3).

3.1. Definition of urban and rural areas and station pairs

3.1.1. Determination of urban and rural areas

In this study, the pixels within urban boundaries provided by the GUB data were flagged as urban areas, and the rural areas were defined as the ring areas between the buffer zones of 1.5 km and 10 km outside the urban edge. The pixels tagged as snow and ice, water bodies, and permanent wetlands were removed to avoid their impacts on the estimation of SUHII (Chakraborty et al., 2020; Chakraborty and Lee, 2019; Lai et al., 2018). In addition, pixels with elevations exceeding ± 50 m from the median elevation of urban pixels were also disregarded to eliminate the impact of altitude (Imhoff et al., 2010; Lai et al., 2018; Venter et al., 2021; Zhang et al., 2014b).

3.1.2. Selection of urban–rural station pairs

In previous studies, CUHII was typically estimated as the T_a difference between a selected urban–rural station pair (Tam et al., 2015; Wang et al., 1990), and the station pairs are generally defined based on the ISP within a buffer zone around the station (Tysa et al., 2019; Wang et al., 2017). In this investigation, we similarly differentiated urban and rural stations by calculating the ISP of a 200-m buffer zone around the station to retrieve urban–rural station pairs, mainly considering that the footprint of a meteorological sensor is roughly 50 to 100 times its height (Oke, 2004; Oke et al., 2017). We complied with the following steps to select appropriate urban–rural station pairs. (1) *Preliminary delineation of urban and rural stations*: Stations with an ISP greater than 20% and within urban boundaries were recognized as urban, while those with an ISP less than 20% as well as within rural boundaries were identified as rural (Wang et al., 2017). Note that the ISP of 20% was used because it is generally used as the division threshold between 'non-urban' and 'low-density urban' surfaces (Homer et al., 2004; Song et al., 2016). (2) *Removal of urban and rural stations along urban–rural edges*: The urban stations close to the urban–rural edges and the rural stations close to the urban areas were removed to improve the representativeness of urban and rural surfaces, respectively. (3) *Further confirmation of urban–rural station pairs*: Although nearly 30,000 stations of T_a measurements are available globally, very few are truly urban, and most cities with urban stations possess only one station within their urban boundaries once filtered by the above two criteria. Nevertheless, very few cities hold more than one station within urban or rural areas; in this case, the urban

station with the largest ISP (highest urbanization level) and the rural station with the smallest ISP (least affected by urbanization) were combined as a station pair (Wang et al., 2017). Following the above filtering procedures, a total of 366 cities were selected globally, including 355 cities in the Northern Hemisphere and 11 cities in the Southern Hemisphere. We acknowledge that uncertainties may occur in the calculation of CUHII by pairing urban and rural stations because of the high heterogeneity in terms of local climate zones (Stewart, 2011; Stewart, 2019; Stewart and Oke, 2012). Nevertheless, usable urban stations, especially on a global scale, remain very limited. A sensitivity analysis of this issue is thus provided in Section 5.2.2.

3.2. Calculation and simultaneous investigation of SUHII and CUHII

3.2.1. Calculation of SUHII and CUHII

The T_s–based SUHII and T_a–based CUHII were calculated using the following formula (Imhoff et al., 2010; Tam et al., 2015):

$$\begin{cases} \text{SUHII} = T_{s\_u} - T_{s\_r} \\ \text{CUHII} = T_{a\_u} - T_{a\_r} \end{cases} \quad (1)$$

where T_{s_u} and T_{s_r} are the mean urban and rural T_s, respectively, and T_{a_u} and T_{a_r} denote the T_a of the associated urban–rural station pairs.

Here, SUHII was calculated based on all the urban and rural pixels, while CUHII was calculated by urban–rural station pairs. Considering these two different definitions, we further calculated $\text{SUHII}_{\text{pixel}}$ based on T_s at the pixels where the station pairs are located, given as:

$$\text{SUHII}_{\text{pixel}} = T_{\text{pixel\_s\_u}} - T_{\text{pixel\_s\_r}} \quad (2)$$

where $T_{\text{pixel\_s\_u}}$ and $T_{\text{pixel\_s\_r}}$ denote the T_s at the pixels where the urban and rural stations are located, respectively. More details on the different representations between SUHII and CUHII are presented in Section 5.2.1.

3.2.2. Simultaneous investigation of SUHII and CUHII

The differences in spatiotemporal patterns between SUHII and CUHII across climate zones were examined simultaneously from the following aspects, including the investigation of (1) SUHII and CUHII for the daytime and nighttime, respectively, (2) day–night difference of SUHII and CUHII, and (3) seasonal variations of SUHII and CUHII.

(1) *SUHII and CUHII for the daytime and nighttime:* Daytime and nighttime SUHII ($\text{SUHII}_{\text{day}}$ and $\text{SUHII}_{\text{ngt}}$) were calculated based on the Aqua/MODIS T_s. Because hourly T_a data are unavailable on a global scale, the monthly mean maximum and minimum T_a were considered as substitutes for the daytime T_a (i.e., $\text{CUHII}_{\text{day}}$) and nighttime T_a (i.e., $\text{CUHII}_{\text{ngt}}$), respectively. We also acknowledge that the acquisition time difference between T_s and T_a may introduce uncertainties into the associated investigations; therefore, a detailed discussion on this issue is given in Section 5.2.3.

(2) *Day–night difference of SUHII and CUHII:* The difference between daytime and nighttime SUHII (ΔSUHII) and CUHII (ΔCUHII), also known as urbanization-induced variations in the diurnal temperature range of T_s (denoted as $\Delta\text{DTR}_{\text{LST}}$) and T_a (denoted as $\Delta\text{DTR}_{\text{SAT}}$) (Huang et al., 2017; Wang et al., 2007), was calculated using the following formula:

$$\begin{aligned} \Delta\text{UHII} &= \text{UHII}_{\text{day}} - \text{UHII}_{\text{ngt}} = \left(T_{\text{u\_day}} - T_{\text{u\_ngt}}\right) - \left(T_{\text{r\_day}} - T_{\text{r\_ngt}}\right) \\ &= \text{DTR}_{\text{u}} - \text{DTR}_{\text{r}} = \Delta\text{DTR} \end{aligned} \quad (3)$$

where UHII_{day} and UHII_{ngt} represent SUHII (CUHII) during the daytime and at night, respectively; $T_{\text{u\_day}}$, $T_{\text{r\_day}}$, $T_{\text{u\_ngt}}$, and $T_{\text{r\_ngt}}$ denote the T_s (T_a) of urban and rural areas during the daytime and nighttime, respectively; DTR_{u} and DTR_{r} are the diurnal temperature ranges of urban and rural areas, respectively; and ΔDTR is the urbanization-induced variation in the diurnal temperature range.

(3) *Seasonal variations in SUHII and CUHII*: The SUHII and CUHII were averaged by season in each city, and the seasonal variations in SUHII and CUHII were investigated in each climate zone for the daytime and nighttime, respectively.

3.3. Examination of controls of SUHII and CUHII

This study mainly examined the impacts from surface properties (i.e., ΔEVI, ΔISP, ΔWSA), overall urbanization metric (expressed by the logarithm of urban population, i.e., log(*P*)) and climatic controls (i.e., T_{max}, T_{min}, PREP) on SUHII and CUHII from both global and climatic perspective, primarily considering their accessibility at a large scale as well as the widespread analysis of these controls in previous studies (Clinton and Gong, 2013; Lai et al., 2021; Li et al., 2020a; Manoli et al., 2019; Peng et al., 2012; Venter et al., 2021; Zhao et al., 2014). Corresponding to the definitions of SUHII and CUHII (Section 3.2.1), the associated ΔEVI, ΔISP, and ΔWSA were calculated based on all the urban and rural pixels and urban–rural station pairs, respectively. Given the unavailability of sub-pixel imperviousness information, the ΔISP corresponding to the station-based CUHII was calculated as the difference in ISP between the 200-m buffer zones of the urban–rural station pairs (Wang et al., 2017). The associated T_{max}, T_{min}, and PREP corresponding to SUHII and CUHII were all derived from the mean value of rural background when investigating the impacts from background climate on these two types of UHIs. We also acknowledge that the different definitions of SUHII and CUHII may introduce additional uncertainties into the investigation of their controls, and more detailed discussions on this issue will therefore be given in Section 5.2.1.

4. Results

4.1. Spatiotemporal pattern of SUHII and CUHII

4.1.1. Spatiotemporal pattern of SUHII

The annual mean SUHII across the selected cities is 1.7 ± 1.5 °C (mean ± Std) during the daytime (Fig. A1) and 1.1 ± 0.8 °C (mean ± Std) at nighttime (Fig. A2), respectively. In addition, the SUHII was higher during the daytime than at night in 65% of the cities. From the zonal perspective, the daytime SUHII averaged for the cities in the equatorial zone is the highest (2.3 °C), followed by that in the warm temperate (2.0 °C) and snow climates (1.9 °C). The daytime SUHII reaches the lowest and is even negative in an arid climate (−0.4 °C). In comparison, at night, the largest SUHII appears in the arid zone (1.8 °C), followed by that in the equatorial (1.4 °C), snow (1.0 °C), and warm temperate climates (0.9 °C). Both daytime and nighttime SUHII are found to be positive in most cities; only 12% of the cities during the day and 7% of the cities at night are characterized by a negative SUHII, that is, the occurrence of surface urban cool island (SUCI). We do not elaborate on the spatiotemporal patterns of SUHII here, as they are mostly consistent with previous findings on a global scale (Chakraborty and Lee, 2019; Clinton and Gong, 2013; Li et al., 2020b; Peng et al., 2012).

4.1.2. Spatiotemporal pattern of CUHII

The annual mean CUHII across all cities was 0.6 ± 1.3 °C (mean ± Std) during the day (Fig. 2) and 0.8 ± 1.4 °C (mean ± Std) at night (Fig. 3), and the nighttime CUHII was higher than the daytime CUHII in 65% of the cities. Increased nighttime CUHII and the higher number of cities at night are anticipated due to the much lower nocturnal cooling rate over urban canyons (Anniballe et al., 2014; Oke et al., 2017; Wong et al., 2011).

During the day, the annual mean CUHII in the warm temperate zone was highest (0.7 °C), followed by that in the snow zone (0.6 °C) and arid zone (0.4 °C), whereas the CUHII reaches its lowest in the equatorial zone (−0.3 °C). Positive CUHII occurs in a large proportion (67%) of

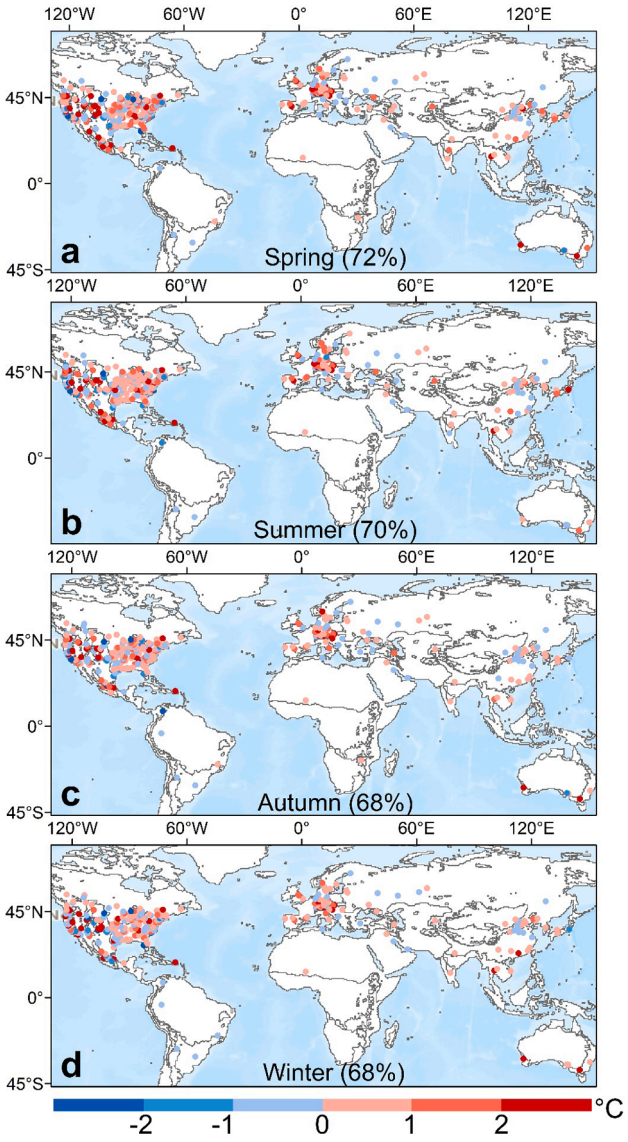

Fig. 2. Spatiotemporal patterns of daytime CUHII in different seasons. The percentages in brackets indicate the proportion of cities with positive CUHII. Spring, summer, autumn, and winter are defined as the period from March to May, June to August, September to November, and December to February respectively across the Northern Hemisphere, while the definition is reversed for the Southern Hemisphere.

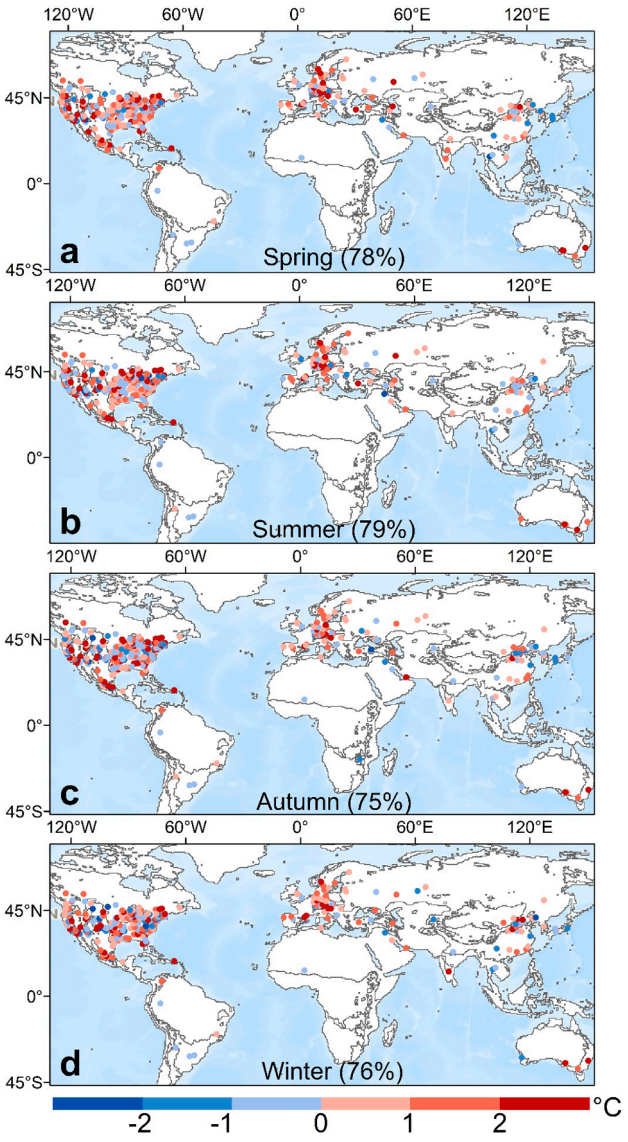

Fig. 3. Spatiotemporal patterns of nighttime CUHII in different seasons.

cities; negative CUHII (i.e., canopy urban cool island, CUCI) appears in a very few cities in the tropics, but it occurs in approximately 30% of the cities in other climate zones. Two reasons could explain the occurrence of CUCI. First, the shading of high-rise buildings in some cities would block daytime solar radiation, especially in the early morning when the solar altitude is low, leading to a slower heating rate on urban surfaces (Chow and Roth, 2006). Second, for some cities, especially in the arid zone, the urban vegetation coverage can be even larger than that over rural bare lands, resulting in reduced urban T_a due to stronger evapotranspiration (Brazel et al., 2000). For example, Chihuahua, a city of Mexico located in the Chihuahua Desert, is characterized by a significant daytime CUCI throughout the year (the annual mean daytime CUHII is −0.4 °C).

At night, the annual mean CUHII in the warm temperate (0.8 °C) and snow zone (0.8 °C) are slightly greater than those in the arid (0.7 °C) and equatorial zone (0.5 °C). While the majority (73%) of cities have positive CUHII, the CUCI was identified in all the climate zones, and the percentages of cities exhibiting a CUCI are relatively higher in the warm temperate (21%), snow (28%), and arid (37%) zones than in the equatorial zone, within which a CUCI is observed only in a few cities. These percentages are relatively high, considering the prevalence of heat islands at the canopy layer at night. One major reason is the use of the monthly mean minimum T_a rather than daily minimum T_a on calm clear-sky days for the calculation of nighttime CUHII, mostly because of the difficulty and even impossibility of obtaining *in situ* hourly urban–rural T_a pairs for hundreds of cities on a global scale (refer to Section 3.1.2). Our identified percentage (27%) of cities with negative nighttime CUHII are on par with (slightly higher) the proportion (16%) of previous identifications that used the monthly mean T_a data to examine CUHIs (Debbage and Shepherd, 2015). Here, the slightly higher percentage may be attributed to the involvement of a greater number of small cities where the CUCI occurs more frequently in the current study when compared with the selection of megacities only in Debbage and Shepherd. (2015). Physically, when using monthly mean data, the higher occurrence of CUCI than anticipated could be a result of incorporating days with heavy rainfall and cloud cover in the wet season, during which the CUCI can be developed (Hu et al., 2019; Morris et al., 2001). We recognize that uncertainties may be induced by using monthly mean data, especially in terms of the SUHI–CUHI investigation. A detailed

sensitivity analysis is provided in Section 5.2.3.

4.2. Simultaneous investigation of spatiotemporal variations of SUHII and CUHII

4.2.1. Simultaneous investigation of seasonal variations of SUHII and CUHII

SUHII and CUHII differ greatly during the day, but they are relatively close at night (Fig. 4). During the day, the seasonal patterns of SUHII are relatively similar across different climate zones, while those of CUHII significantly depend on the climate zone. At night, the seasonal patterns for SUHII and CUHII were both dependent on the climate zone.

During the day, the annual mean SUHII is higher than CUHII by 1.1 ± 1.9 °C (mean ± Std) across selected cities (Fig. 4a). The difference between SUHII and CUHII is largest in the equatorial zone (2.6 °C on average), followed by the warm temperate zone (1.4 °C) and snow zone (1.3 °C). We observed an opposite phenomenon for cities in the arid climate, under which the CUHII becomes higher than SUHII by 0.8 °C (refer to Rectangle A in Fig. 4a). The reversed urban–rural contrast in vegetation abundance in the arid and semi-arid regions may contribute to the lower SUHII through the appearance of significant daytime SUCI (Huang et al., 2017). Furthermore, the difference between the SUHII and CUHII averaged for all the chosen cities reaches a maximum in summer (2.2 °C) and minimum in winter (0.4 °C), mainly because of the stronger solar radiation associated with a greater urban–rural difference in vegetation coverage in summer, which enlarges the difference between T_s and T_a (Sun et al., 2015; Wang et al., 2017).

At night, SUHII and CUHII are much closer. The annual mean nighttime SUHII is higher than CUHII by only 0.3 ± 1.5 °C (mean ± Std) (Fig. 4b). This difference is the largest in the arid zone (1.1 °C), followed by the equatorial zone (0.8 °C), and is relatively small in the snow zone (0.3 °C) and warm temperate zone (0.1 °C). Similarly, the difference in nighttime SUHII and CUHII was also largest in summer (0.5 °C) and smallest in winter (−0.01 °C). Note that the differences between SUHII and CUHII during both the day and at night quantified here are generally analogous to several previous studies conducted at a large scale (Venter et al., 2021; Zhang et al., 2014b), which further verifies the reliability of our findings. Nevertheless, there are truly slight differences between these two types of UHIIs obtained in this study and those in Venter et al. (2021) (i.e., the differences between SUHII and CUHII quantified here are slightly lower). The discrepancy in dataset and study area, together with the augmented UHIIs during heat wave periods (Zhao et al., 2018), might contribute to such slight differences.

In terms of seasonal patterns, the summer daytime SUHII reaches the strongest for all the climate zones (Fig. 4a), while the seasonal variations of daytime CUHII are diverse across climate zones (Fig. 4a). In the equatorial zone, CUHII was stronger in spring and winter than in summer and autumn. In the arid zone, CUHII reached the maximum and minimum values in summer and winter, respectively. The seasonal variations of CUHII in the warm temperate and snow zones were very small (with an amplitude of variation less than 0.2 °C). At night, the seasonal patterns of SUHII significantly depend on the climate zone (Fig. 4b). The SUHII in the warm temperate and snow zones reach the strongest in summer and the weakest in winter, while in the equatorial zone, maximum and minimum SUHII occurs in summer and autumn respectively. For the arid zone, the strongest SUHII is observed in spring. The seasonal dynamics of CUHII also differed in various zones (Fig. 4b). For CUHII, its maxima and minima occur in summer and winter respectively in both warm temperate and snow zones, whereas in arid zone, spring and autumn possess the maxima and minima respectively. In the tropics, CUHII was significantly lower in summer than in other seasons (Fig. 4b).

4.2.2. Simultaneous investigation of diurnal variations of SUHII and CUHII

The diurnal variations (i.e., day–night difference) of the SUHII (i.e., ΔSUHII) and CUHII (ΔCUHII) across climate zones are displayed in Fig. 5. As indicated in Section 3.2.2, the ΔSUHII and ΔCUHII are equivalent to the urbanization-induced variations in the T_a– and T_s–based DTR (i.e., ΔDTR_{LST} and ΔDTR_{SAT}), respectively (Huang et al., 2017; Wang et al., 2007).

The annual mean ΔSUHII and ΔCUHII averaged across all the selected cities are 0.6 ± 1.8 °C (mean ± Std) and −0.2 ± 1.6 °C (mean ± Std), respectively, implying that urbanization leads to an increase in DTR_{LST} and a decrease in DTR_{SAT} (Fig. 5). However, we observe the opposite phenomenon for cities in an arid climate, which is characterized by a negative annual mean ΔCUHII (−0.2 °C) along with a negative ΔSUHII (−2.2 °C) (Rectangular A in Fig. 5). The discrepancy between arid and other climates may again be attributable to the greater vegetation abundance in urban areas than in rural areas in arid climates (Huang et al., 2017). From a seasonal perspective, the seasonal variations of ΔSUHII are significant, characterized by a high ΔSUHII in summer across almost all climate zones, while the seasonal patterns of

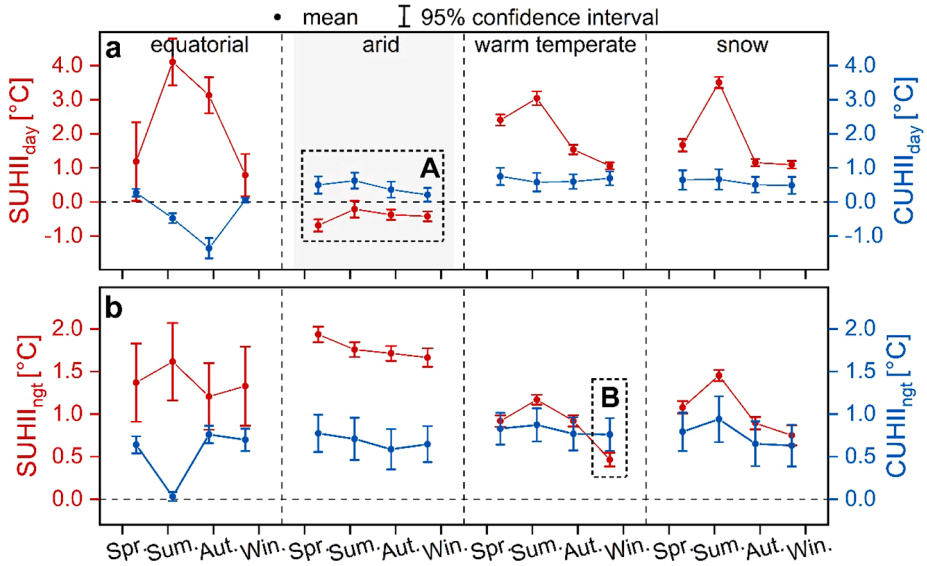

Fig. 4. Seasonal variations of SUHII (red) and CUHII (blue) during day (**a**) and night (**b**) across different climate zones. (For interpretation of the references to colour in this figure legend, the reader is referred to the web version of this article.)

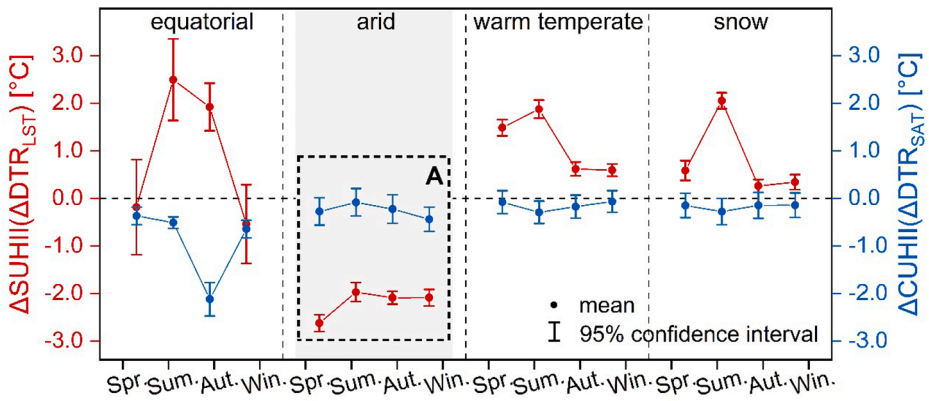

Fig. 5. Seasonal variations of ΔSUHII (red) and ΔCUHII (blue) across various climate zones. (For interpretation of the references to colour in this figure legend, the reader is referred to the web version of this article.)

ΔCUHII are inconsistent for cities in different climate zones (Fig. 5). In the equatorial zone, ΔCUHII is significantly lower in autumn than in other seasons; in the arid zone, ΔCUHII is the strongest in summer and weakest in winter, whereas in the warm temperate and snow zones, the seasonal variations of ΔCUHII are very small, with an amplitude of variation less than 0.15 °C.

4.3. Simultaneous examination of impacts from controls on SUHII and CUHII

4.3.1. Simultaneous examination of impacts from controls on SUHII and CUHII across the globe

The impacts from surface properties (ΔEVI, ΔISA, and ΔWSA), population size, and climatic controls (T_{max}, T_{min}, and PREP) on SUHII

		ΔEVI	ΔISP	ΔWSA	log(*P*)	T_{max}	T_{min}	PREP
$SUHII_{day}$	Spr.	-0.53**	-0.08	0.28**	0.05	-0.17**	-0.01	0.48**
	Sum.	-0.68**	0.01	0.30**	0.10	-0.38**	-0.15**	0.39**
	Aut.	-0.56**	-0.09	0.44**	0.15**	-0.01	0.11*	0.45**
	Win.	-0.12*	-0.02	-0.08	-0.01	-0.15**	-0.08	0.38**
	Ann.	-0.51**	-0.05	0.35**	0.09	-0.18**	-0.03	0.61**
$CUHII_{day}$	Spr.	-0.03	0.04	0.18**	0.09	-0.01	-0.08	-0.10
	Sum.	-0.11*	0.07	0.24**	0.04	-0.08	-0.17**	0.05
	Aut.	-0.05	0.10	0.13*	0.08	-0.05	-0.09	-0.04
	Win.	-0.07	0.05	-0.04	0.12*	0.00	0.02	0.03
	Ann.	-0.12*	0.10	0.03	0.15*	-0.05	-0.07	-0.02
$SUHII_{ngt}$	Spr.	0.04	0.12*	-0.21**	0.41**	0.23**	0.11*	-0.36**
	Sum.	-0.14**	0.08	-0.26**	0.37**	0.13*	0.05	-0.14**
	Aut.	-0.03	0.10	-0.30**	0.37**	0.23**	0.14**	-0.30**
	Win.	-0.04	0.14**	-0.36**	0.37**	-0.05	-0.15**	-0.41**
	Ann.	-0.07	0.13*	-0.34**	0.43**	0.10	0.03	-0.31**
$CUHII_{ngt}$	Spr.	-0.23**	0.17**	-0.02	0.19**	-0.08	-0.08	-0.08
	Sum.	-0.31**	0.21**	-0.02	0.17**	-0.10	-0.12*	-0.04
	Aut.	-0.21**	0.13*	0.09	0.17**	-0.02	0.00	-0.03
	Win.	-0.18**	0.08	-0.06	0.19**	-0.01	0.02	-0.02
	Ann.	-0.38**	0.18*	-0.09	0.25**	-0.04	0.00	-0.01

Fig. 6. Statistical significance (denoted by the correlation coefficient *r*) between various controls and the SUHII and CUHII during the day and night in spring (Spr.), summer (Sum.), autumn (Aut.), winter (Win.), and across the annual (Ann.) cycle. The asterisk (*) indicates statistical significance at the 0.05 level, and (**) suggests statistical significance at the 0.01 level.

and CUHII across the globe are shown in Figs. 6 and 7, respectively. The results show that these controls exert different impacts on these two types of UHIs.

In terms of ΔEVI and ΔISP, both SUHII and CUHII are negatively correlated with ΔEVI and positively correlated with ΔISP in general, although the associated statistical significance is different. Specifically, during the day, ΔEVI exerts a larger impact on SUHII ($r = -0.51$, $p < 0.01$) than on CUHII ($r = -0.12$, $p < 0.05$), while the relationships between ΔISP and CUHII ($r = 0.10$) and SUHII ($r = -0.05$) are both insignificant. At night, both the impacts of ΔEVI and ΔISP on CUHII ($r = -0.38$, $p < 0.01$ and $r = 0.18$, $p < 0.05$, respectively) are greater than those on SUHII (r: −0.07, and 0.13, respectively) (Fig. 6). Although vegetation coverage and ISP are highly correlated (Ridd, 1995), we observe that their impacts on SUHII and CUHII are not entirely identical. We speculate that this is likely because vegetation coverage regulates the UHI mainly by its enhanced evapotranspiration capacity (Elmes et al., 2017; Sun et al., 2015), while ISP regulates the UHI through building geometry in addition to its decrease in evapotranspiration in contrast to vegetation coverage (Mirzaee et al., 2018).

In terms of ΔWSA, there were significant correlations between SUHII and ΔWSA, with a positive relationship ($r = 0.35$, $p < 0.01$) during the day and a negative relationship ($r = -0.34$, $p < 0.01$) at night (Fig. 6), which is consistent with previous studies at the global scale (Peng et al., 2012). By comparison, CUHII possesses a weak positive and negative correlation with ΔWSA during the day ($r = 0.03$) and at night ($r = -0.09$) respectively (Fig. 6).

In terms of population size, both SUHII and CUHII are, in general, positively correlated with log(P) during the day and night. During the day, the impacts from log(P) on both SUHII and CUHII are relatively small and the former ($r = 0.09$) is slightly weaker than that the latter ($r = 0.15$, $p < 0.05$) (Fig. 6). With the increase in population size, the annual daytime SUHII first decrease and then increase, whereas the CUHII holds the opposite situation (Fig. 7e). At night, log(P) exerts a significantly larger impact on both SUHII and CUHII than during the day ($r = 0.43$ and 0.25 respectively, $p < 0.01$) (Fig. 6). With the increase in population size, the annual nighttime SUHII steadily increased, while the annual nighttime CUHII did not (Fig. 7e). Our identified correlations between CUHII and log(P) are relatively weaker than those in previous studies such as Oke (1973), which can be due to the use of monthly mean T_a data rather than measurements under ideal conditions (i.e., calm and clear nights).

Interestingly, the impacts of population size on daytime SUHII turn into negative in winter, and notably, a larger population size can be accompanied by a smaller daytime SUHII (Fig. 7d). The occurrence of the SUCI over a part of megacities (e.g., Beijing) in winter as a result of the transition of rural background from vegetation surfaces (crops) into bare soil (due to crop harvesting) may contribute to this reversed phenomenon (Huang et al., 2017).

In terms of climatic controls, the impacts of T_{max} and T_{min} on the UHIIs are similar. For example, there is a negative relationship between T_{max} and these two types of UHIIs during the day, yet with a larger influence on SUHII ($r = -0.18$, $p < 0.01$), while the relationships between T_{max} and SUHII and CUHII are both insignificant at night. For PREP, the significant positive correlation between the annual mean PREP and SUHII during the day ($r = 0.61$, $p < 0.01$) and the associated negative correlation during the night ($r = -0.31$, $p < 0.01$) are generally consistent with previous studies (Lai et al., 2021; Peng et al., 2012; Zhao et al., 2014). This is mainly due to the significantly decreased rural surface temperature with higher soil moisture after precipitation (He, 2018). In contrast, the relationships between PREP and CUHII are very weak both during the day and at night.

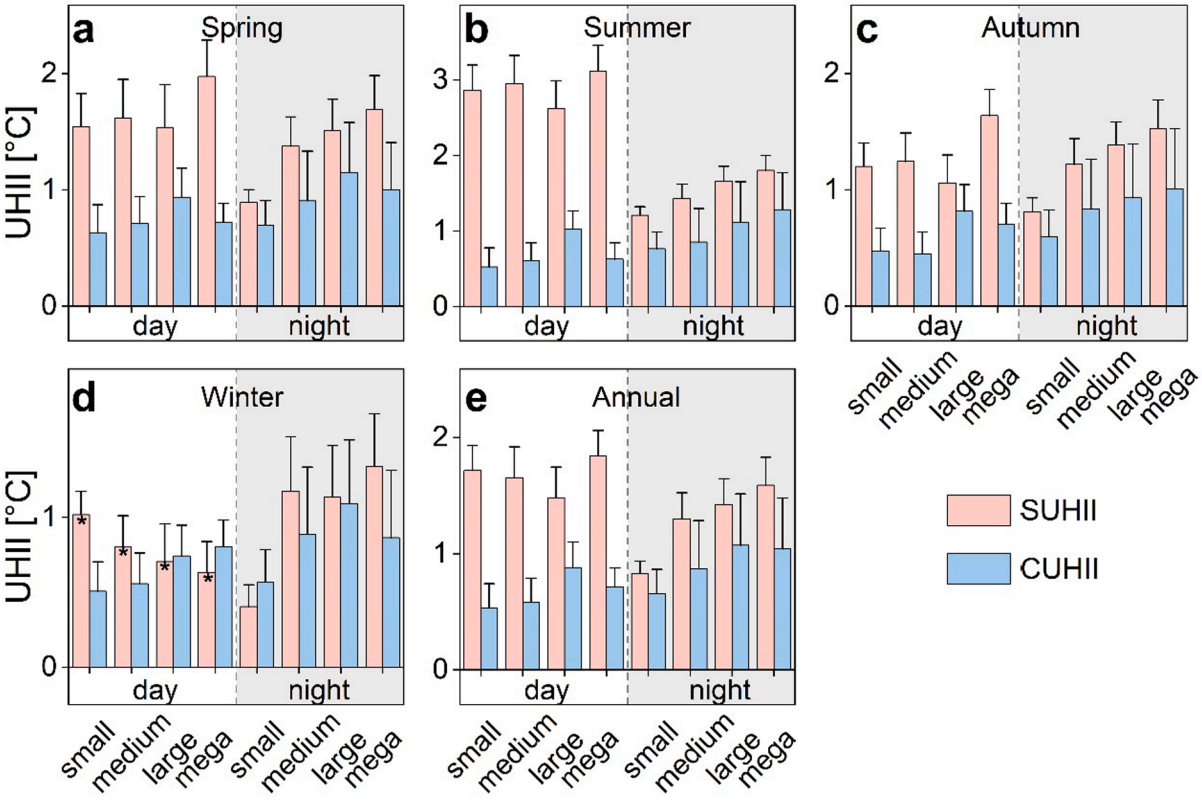

Fig. 7. Changes in SUHII and CUHII along with population size. The cases for the seasonal UHI intensities are provided in (**a**) to (**d**) while that for the annual mean is given in (**e**). The label * is used to highlight the negative relationship between the winter daytime SUHII and population size contrasting with the positive one for the other cases. The bar indicates the upper end of the 95% confidence interval.

4.3.2. Simultaneous examination of impacts from controls on SUHII and CUHII across various climates

The impacts from surface properties (i.e., ΔEVI, ΔISP, and ΔWSA), overall urbanization metric (i.e., log(*P*)), and climatic controls (i.e., T_{max}, T_{min}, and PREP) on SUHII and CUHII across the arid, warm temperate, and snow climates were further analyzed (Tables S1, S2, and S3). Note that the results for equatorial climate were not included due to the weak correlation coefficients ($p < 0.05$) between controls and SUHII/CUHII over such a zone owing to the small number of cities (only 10 cities).

The results indicate that the impacts from the above controls on the two types of UHIIs are affected by background climate. Specifically, for ΔEVI, the annual mean ΔEVI exerts a larger impact on SUHII than on CUHII during the day in all three climates, whereas at night, it influences CUHII more in warm temperate and snow zones but influences SUHII more in arid climate. As to ΔWSA, the relationship between the annual mean ΔWSA and SUHII during the day is positive in all these three climatic zones; while at night it becomes opposite in warm temperate and snow zones. The relationship between ΔWSA and CUHII is significantly negative only at night in snow climate. For PREP, its impacts on SUHII are similar in warm temperate and snow climates (i.e., positive during the day yet negative at night), while the arid zone holds a different situation (i.e., positive at both day and night). In contrast, the relationships between the annual mean PREP and CUHII are insignificant in all climates both during the day and at night.

5. Discussion

5.1. Clarifications and perspectives

The SUHI and CUHI are two distinctly different yet complementary components of the UHI effect (Manoli et al., 2020b; Martilli et al., 2020b). The simultaneous investigation of these two types of UHIs can help comprehensively describe the vertical structure of UHI and can better reflect urban surface-atmosphere interaction, which is critical for a better understanding of urban surface energy budget (Jin, 2012; Venter et al., 2021). Furthermore, considering both SUHI and CUHI are closely related to thermal comfort, the simultaneous investigation of these two can also help better evaluate urban thermal environment (Venter et al., 2021; Wang et al., 2020).

In the past few years, the simultaneous investigation of SUHI and CUHI has received more attention in the urban climate community (Anniballe et al., 2014; Chakraborty et al., 2017; Ho et al., 2016; Hu et al., 2019; Venter et al., 2021; Wang et al., 2020; Yang et al., 2020; Zhang et al., 2014b). Nonetheless, these previous studies have mainly focused on a limited number of cities and/or background climates, mostly due to the difficulty of obtaining consistent urban T_a measurements over global cities. In other words, the differences in the spatio-temporal variations between SUHI and CUHI remain largely not clear over global cities. Besides, the dissimilar impacts of various typical controls on these two types of UHIs have not been elucidated adequately across various background climates at a global scale.

This study compared SUHI and CUHI over global cities by selecting appropriate urban–rural station pairs consistently from nearly 30,000 meteorological stations across the globe. The meteorological dataset as well as the used strategy for filtering urban–rural station pairs are expected to be useful to provide a reliable data source for future urban climate studies related to CUHI and the SUHI–CUHI comparison across the globe. This current investigation differs from previous SUHI–CUHI comparison studies in that (1) we incorporated hundreds of cities within a great variety of background climates worldwide as well as in that (2) we examined the statistical relationships between SUHII/CUHII (especially CUHII) and several types of controls (e.g., surface property, background climate, and urban population) over global cities.

Practitioners may suggest that the global (or large-scale) SUHI–CUHI investigation may be achievable based on global T_a estimates that are modeled based on a series of predictors, including satellite T_s data. However, the SUHI–CUHI comparison can likely be impacted and even distorted based on the combination of satellite T_s data and modeled T_a data, which are now closely related to the satellite T_s data. Therefore, consistent urban T_a observations for cities over a large spatial scale are necessary to facilitate the SUHI–CUHI comparison. It has been noticed that a small part of the T_a measurements from the Global Historical Climatology Network were installed over surfaces with a high ISP and can therefore be perceived as urban stations, based on which the SUHI–CUHI comparison could be conducted (Zhang et al., 2014b). Nevertheless, this previous large-scale study only focused on continental United States. A very recent study demonstrated that consistent urban T_a observations could also be obtained from crowdsourced data (Venter et al., 2021), yet this study only focused on cities in Europe, where arid and equatorial climates are mostly absent. It is also worthy to note that, though with different types of T_a measurements, some of our findings echo well with those by Venter et al. (2021). For example, this study and Venter et al. (2021) gained a similar finding that SUHII is significantly larger than CUHII during the day while the former one is only marginally greater than its counterpart at night.

Considering the different characteristics of satellite T_s and *in situ* T_a data, we acknowledge that uncertainties may exist in this study. First, the use of different definitions between SUHII and CUHII may affect the SUHI–CUHI investigation. Second, the calculation of CUHII may not be adequately accurate by limited urban–rural station pairs of T_a data. Finally, the SUHI–CUHI investigation may also be affected by the acquisition time difference between T_s and T_a, as well as the time difference of measuring T_a in urban and rural stations (because the times at which they reach the monthly mean maximum and minimum differ). More sensitivity analysis related to the issues presented above is provided as below.

5.2. Sensitivity analysis

5.2.1. Impacts from different definitions between SUHII and CUHII

In this study, SUHII was calculated based on all urban and rural pixels, mostly because the overall SUHI can be better represented by this approach than by using only the pixels at the locations of station pairs due to the high heterogeneity of urban surfaces (Stewart, 2011; Stewart, 2019; Stewart and Oke, 2012). This is also because of the widespread acceptance of using all available urban and rural pixels to calculate the SUHII (Clinton and Gong, 2013; Peng et al., 2012). Here, CUHII was estimated using urban–rural station pairs. This sampling difference may affect the SUHI–CUHI investigation. Thus, we conduct a sensitivity analysis by additionally calculating SUHII based only on the T_s of the pixels where the station pairs are located (termed $SUHII_{pixel}$) (Fig. 8). The results show that the annual mean $SUHII_{pixel}$ is noticeably greater than SUHII during the day while it is only slightly higher than SUHII at night, mainly because the calculation of $SUHII_{pixel}$ only incorporated a pixel pair with a large ISP value (for the urban station pixel) and a low ISP value (for the rural station pixel). This indicates that the different SUHII definitions would exert a certain impact on the numerical difference between the SUHII and CUHII. For example, the annual mean $SUHII_{pixel}$ is higher than SUHII by approximately 0.9 °C and 0.1 °C during the daytime and at night, respectively, so when compared with the SUHII, the annual mean differences between $SUHII_{pixel}$ and CUHII are relatively higher, which are 2.0 °C during the day (i.e., 1.1 °C + 0.9 °C) and 0.4 °C at night (i.e., 0.3 °C + 0.1 °C); and the annual mean ΔSUHII (ΔDTR_{LST}) based on the T_s of the designated pixels only is also greater (i.e., 1.4 °C). Despite these differences in magnitude, we note that the diurnal and seasonal patterns of the SUHII and $SUHII_{pixel}$ remain hardly changed, and the issue related to such a sampling barely affects the diurnal and annual behaviors of the SUHI.

The different definitions of these two types of SUHII may also affect the examination of their controls, we therefore analyzed such uncertainties by comparing the statistical relationships between the

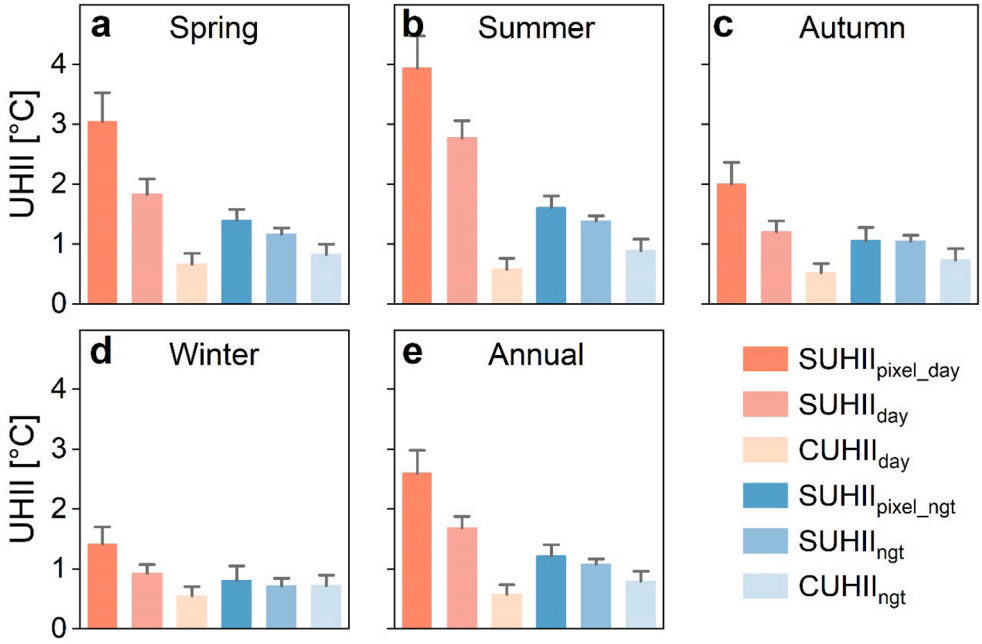

Fig. 8. Seasonal (**a**-**d**) and annual mean (**e**) SUHII$_{pixel}$, SUHII, and CUHII for all cities. The bar indicates the upper end of the 95% confidence interval.

controls and the two types of SUHIIs (i.e., SUHII and SUHII$_{pixel}$) (Fig. 9). The results indicate that, for most of the controls (i.e., ΔEVI, ΔWSA, log (P), T_{max}, T_{min}, and PREP), there are only numerical differences in the correlation coefficient (r) and their signs (i.e., positive or negative) are basically consistent when using either SUHII$_{pixel}$ or SUHII for analysis; while for ΔISP, both the r value and its sign can be different. This suggests that the different SUHII definitions would also exert a certain impact on the examination of the controls of SUHII and CUHII, especially for ΔISP.

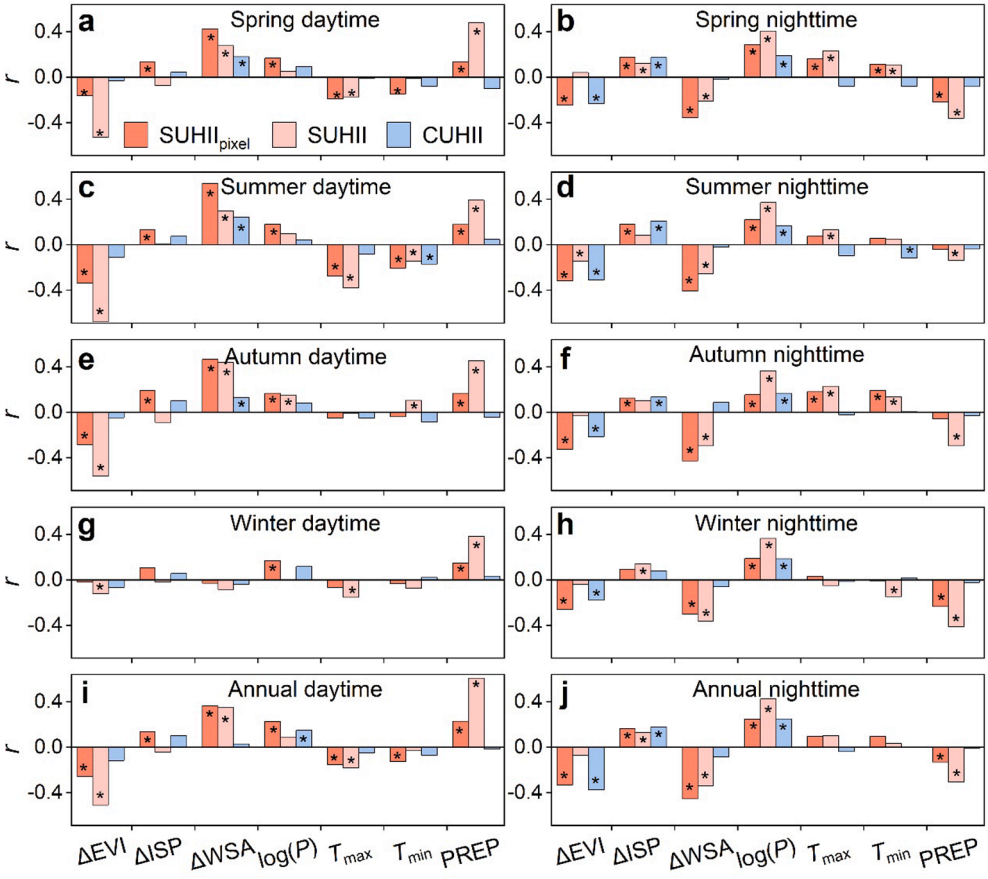

Fig. 9. Statistical significance (r) between various controls and SUHII$_{pixel}$, SUHII, and CUHII. The asterisk (*) indicates statistical significance at the 0.05 level.

5.2.2. Impacts from insufficient representativeness of urban–rural station pair

The criteria adopted for selecting urban–rural station pairs in this investigation include: (1) whether the station is within the urban or rural boundary and (2) whether the ISP in a 200-m buffer zone around the station is greater or less than 20%. Note that the locations of the station pairs may largely affect the representativeness of urban or rural T_a and, therefore, the estimation of CUHII (Stewart, 2011; Stewart, 2019).

To evaluate the representativeness of station pairs, we designed two indicators: (1) the ISP difference in the 200-m buffer zone around the station pairs (ΔISP), and (2) the ratio of distance between the urban and rural stations to the urban center (ΔDist%) (Fig. 10). A larger ΔISP means a greater difference in urbanization level between the station pairs and thus a better representativeness for urban–rural contrast. Similarly, a smaller ΔDist% indicates a shorter distance between the urban station and urban center and a longer distance between the rural station and urban center, which also suggests a better representativeness of the station pairs. To display the representativeness of the selected station pairs, we visually present the locations of the urban–rural station pairs and their surrounding ISPs in a part of the case cities with high-resolution images obtained from Google Earth (Fig. 11). The results in Figs. 10 and 11 show that most urban–rural station pairs possess a relatively large ΔISP along with a fairly small ΔDist%, implying the high representativeness of the station pairs. Specifically, the average ΔISP of all cities is 0.73 ± 0.21 (mean ± Std) with a minimum of 0.14; and the average ΔDist% of all cities is 0.30 ± 0.22 (mean ± Std) with a minimum of 0.84. Lincoln, for example, has a ΔISP of 1.0, with its urban station close to the urban center and a rural station at the edge of its rural background (Fig. 11).

Despite the relatively high representation of the chosen urban–rural station pairs in this study, the dichotomy division of urban–rural surfaces may still have shortcomings (Stewart and Oke, 2012). Therefore, we further resort to hourly T_a data from abundant and densely distributed stations in three case megacities (i.e., Beijing, Shenyang, and Guangzhou, all with > 100 stations (see Section 2.2.1) within different climate zones to further verify the uncertainties. The CUHII calculated by a large number of urban–rural station pairs is hypothesized to be the true value, based on which the uncertainty of CUHII estimated from a randomly selected urban–rural station pair is quantified. The detailed steps for the uncertainty analysis are as follows: (1) *Delineation of urban and rural stations*: according to the ISP threshold (20%) set in Section 3.1.2, 116 urban and 26 rural stations, 73 urban and 15 rural stations, 138 urban and 24 rural stations were retrieved in Beijing, Shenyang, and Guangzhou, respectively. (2) *Calculation of true and possible observation values of CUHII*: we first obtained various observation station pairs by a random combination of all the available urban and rural stations and acquired 3016 (116 × 26), 1095 (73 × 15), and 3312 (138 × 24) station pairs for these three cities, respectively. The true value is then denoted by averaging the CUHII of all station pairs, and the observation values are denoted by the CUHII of randomly selected station pairs. (3) *Estimation of uncertainty with standard deviation (δ)*: in each city, the uncertainty of CUHII with limited station pairs is represented by the standard deviation. A smaller δ generally denotes less deviation and, accordingly, a higher representativeness of each station pair.

The true values and standard deviations of CUHII for these three cities are presented in Fig. 12 a-c. The standard deviations (δ) are mostly within ± 1.5 °C both during the day and at night in these three cities. This deviation is nonnegligible for the calculation of CUHII and for the SUHI–CUHI investigation for a single city. However, it would hardly induce a large bias for the SUHII-CUHII investigation for dozens of and hundreds of cities on a global scale that our study focused on. This is mostly because the conclusions of this study are obtained by averaging the CUHII over all cities randomly distributed in various geographic environments; according to statistical theory, the δ of CUHII for n cities ($\sqrt{\frac{\sum(\delta-\bar{\delta})^2}{n-1}}$) would be much smaller than the δ for a single city (Pugachev, 2014). For example, the δ for all cities within the arid zone (n = 43) and snow zone (n = 110) would be less than 0.04 °C or even much lower, assuming that the δ of using a single urban–rural station pair for a single city is 1.5 °C.

5.2.3. Impacts from data acquisition time differences

The SUHI–CUHI investigation may also be impacted by the possible uncertainties induced by data acquisition time differences by using satellite-derived T_s and *in situ* monthly mean T_a. (1) The acquisition

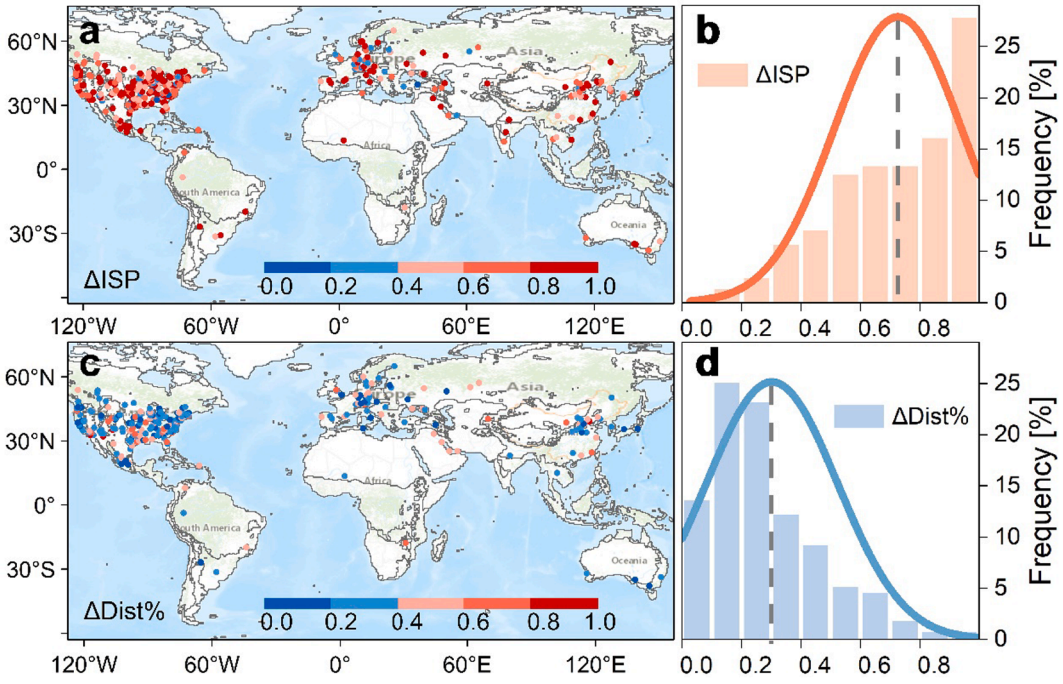

Fig. 10. The spatiotemporal patterns and the frequency histogram of the ΔISP (**a-b**) and the ΔDist% (**c-d**) between urban–rural station pairs. The solid curves are the fitted normal distributions, and the short-dashed lines represent the associated means.

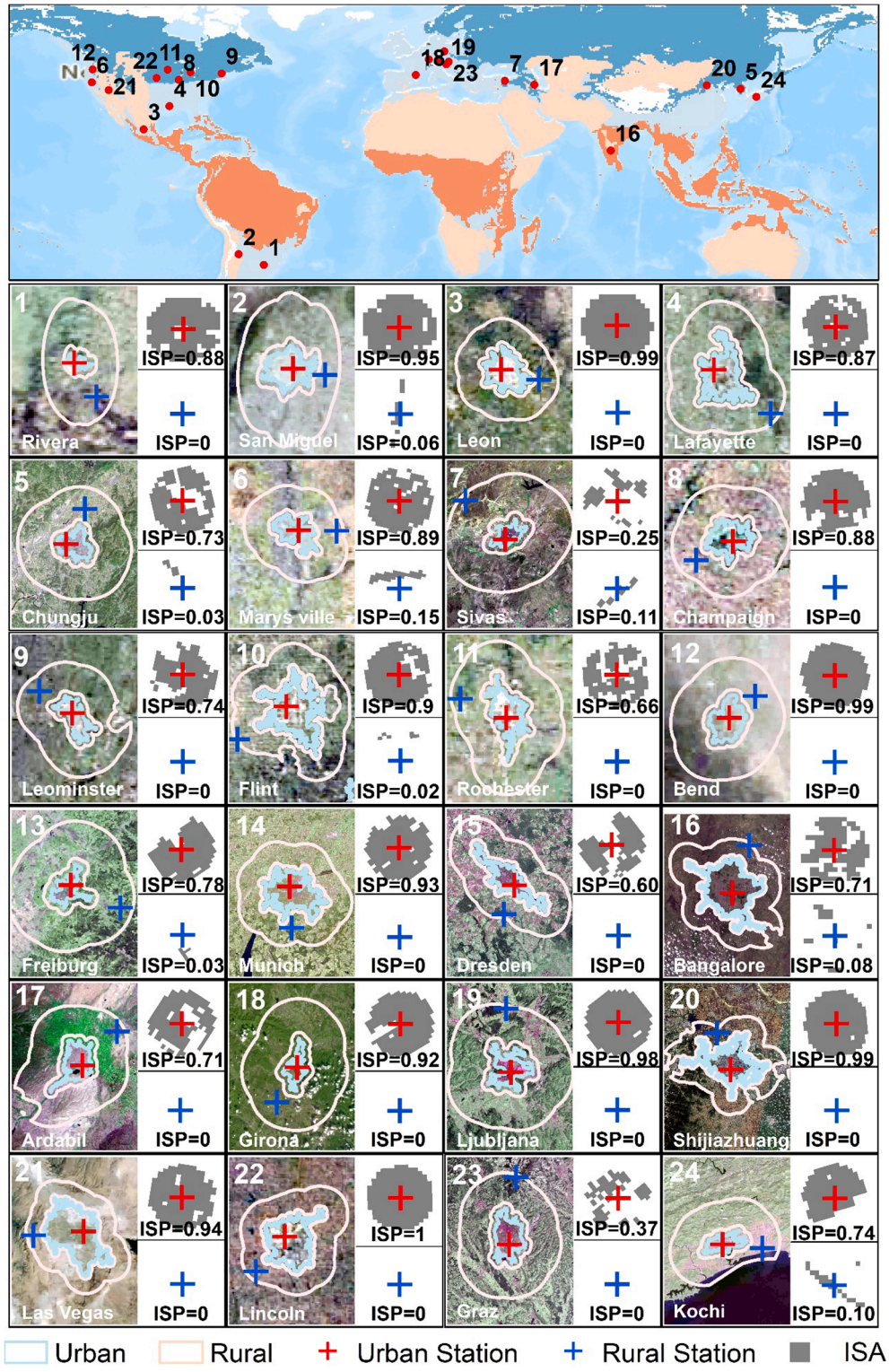

Fig. 11. Locations of urban–rural station pairs and their surrounding ISPs in a part of the chosen cities, with the upper subfigure presenting the locations of these cities.

times of the Aqua/MODIS daytime and nighttime T_s are approximately 13:30 pm and 01:30 am, respectively; while those of the maximum and minimum) T_a are about 14:00 pm and 06:00 am, respectively. This means that there are acquisition time differences between the satellite T_s and *in-situ* T_a both for the day and at night. Such time differences for daytime and nighttime were termed δh_1 and δh_2, respectively. (2) There may also be a time difference between the daily maximum (or minimum) T_a between urban and rural areas. These daily extreme T_a values between urban and rural areas are termed δh_3 and δh_4, respectively.

Here, we again analyze the uncertainties induced by the data acquisition time differences with the hourly T_a from densely distributed stations over the three megacities, including Beijing, Shenyang, and Guangzhou (Fig. 12 d-f). In terms of the acquisition time difference

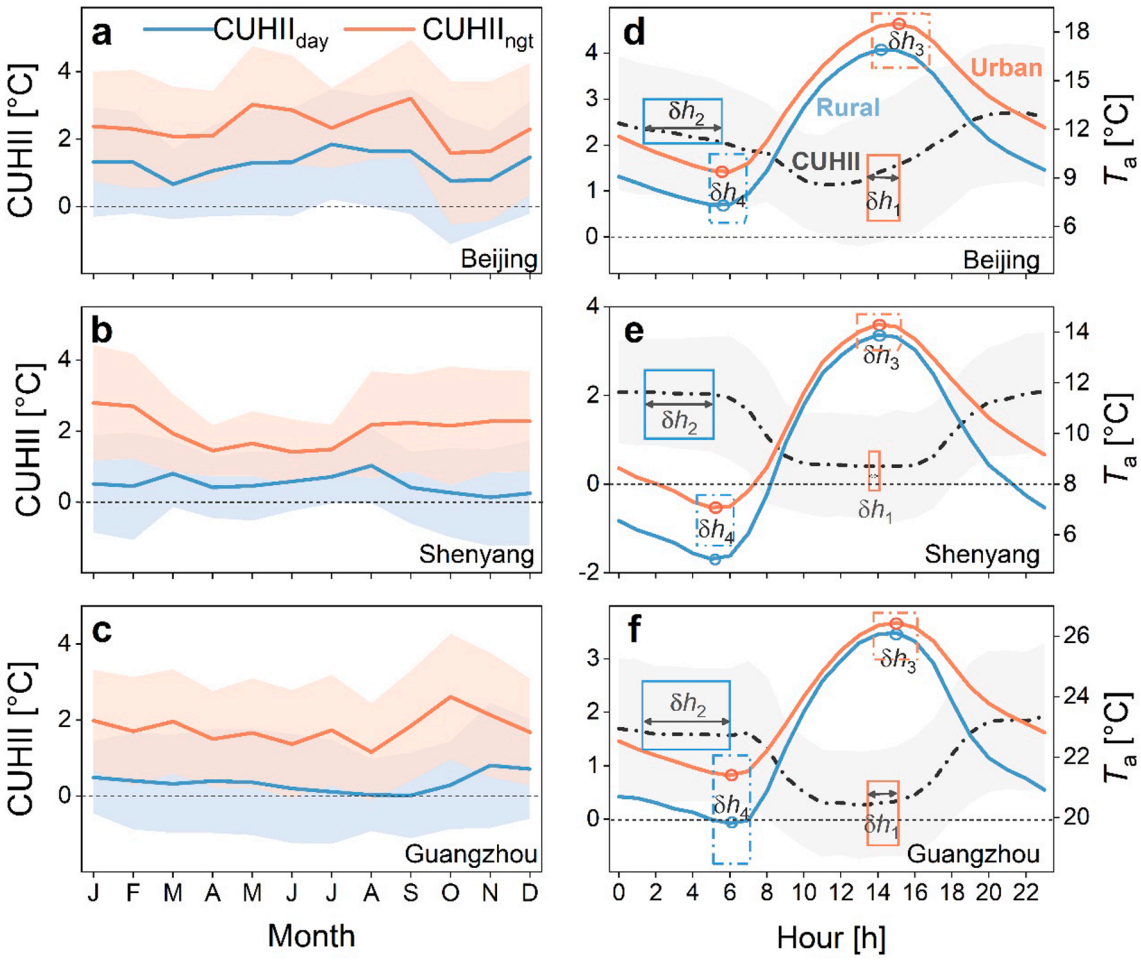

Fig. 12. Monthly variations of CUHII in Beijing (**a**), Shenyang (**b**), and Guangzhou (**c**); and the associated hourly variations of the CUHII and T_a in urban and rural stations over these three megacities (**d-f**). The lines represent the CUHII calculated based on all usable station pairs, while the shades represent the standard deviations of CUHII calculated based on randomly selected single station pairs.

between the satellite-derived T_s and *in situ* T_a, during the δh_1 and δh_2 period (i.e., the period from the time of the daily maximum T_a to the daytime satellite overpass, and from the time of the daily minimum T_a to the nighttime satellite overpass, respectively), there is almost no variation in CUHII in Shenyang and Guangzhou (i.e., the amplitude of variation is less than 0.05 °C), and therefore, the acquisition time difference between T_s and T_a would barely affect the simultaneous investigation of SUHII and CUHII in these two cities. For Beijing, the amplitude of variation of CUHII is relatively higher (0.24 °C for daytime and 0.21 °C for nighttime, refer to the orange solid box and blue solid line box in Fig. 12 d-f). Although CUHII in some cities such as Beijing may be affected by δh_1 and δh_2, their impacts are anticipated to be significantly reduced by averaging the values of all cities for each climate zone and/or on a global scale, as indicated in Section 5.2.2.

In terms of δh_3 and δh_4 (i.e., the time difference of daily extreme T_a between urban and rural areas), it is apparent that δh_4 is very small and therefore exerts little impact on CUHII in all three cities (refer to the blue dashed box in Fig. 12 d-f). The δh_3 is also very small in Shenyang and Guangzhou, yet it is about 1 h in Beijing and its impact on the CUHII can be up to 0.17 °C (refer to the orange dashed box in Fig. 12 d-f). Once more, the relatively greater biases induced by δh_3 were suppressed significantly by averaging the CUHII spatially and temporally.

We also acknowledge that the SUHII derived from MODIS T_s under clear-sky conditions and the CUHII calculated from T_a under all-weather conditions may introduce uncertainties for the SUHI–CUHI investigation. However, it is extremely difficult and even impossible to acquire hourly or daily T_a measurements from densely distributed urban stations on a global scale, and this uncertainty has not yet been analyzed.

6. Conclusion

Previous comparisons of the SUHI and CUHI are mostly limited to a single or few cities, and their associated spatiotemporal patterns and controls under various background climates, especially on a global scale, remain largely unknown. This study investigated the similarities and dissimilarities between SUHII and CUHII in terms of spatiotemporal variations and various controls over 366 global cities. The main conclusions are as follows:

First, the annual mean SUHII is higher than CUHII by 1.1 ± 1.9 °C (mean ± Std) during the day and 0.3 ± 1.5 °C (mean ± Std) at night. The difference between SUHII and CUHII reaches the greatest in the summer (i.e., 2.2 °C and 0.4 °C for the day and night, respectively) while the lowest in winter (i.e., 0.5 °C and −0.01 °C for the day and night, respectively). The differences between SUHII and CUHII are also regulated by background climate, and the differences between SUHII and CUHII for cities in the equatorial, warm temperate, and snow climates are generally consistent with those of the global mean. However, the opposite phenomenon occurs during the day for cities in arid climate, where SUHII is lower than CUHII by 0.8 °C, possibly due to the significant surface urban cool islands resulting from the higher vegetation coverage in urban than in rural areas over arid regions. The sensitivity analysis further indicates that, when compared with the SUHII

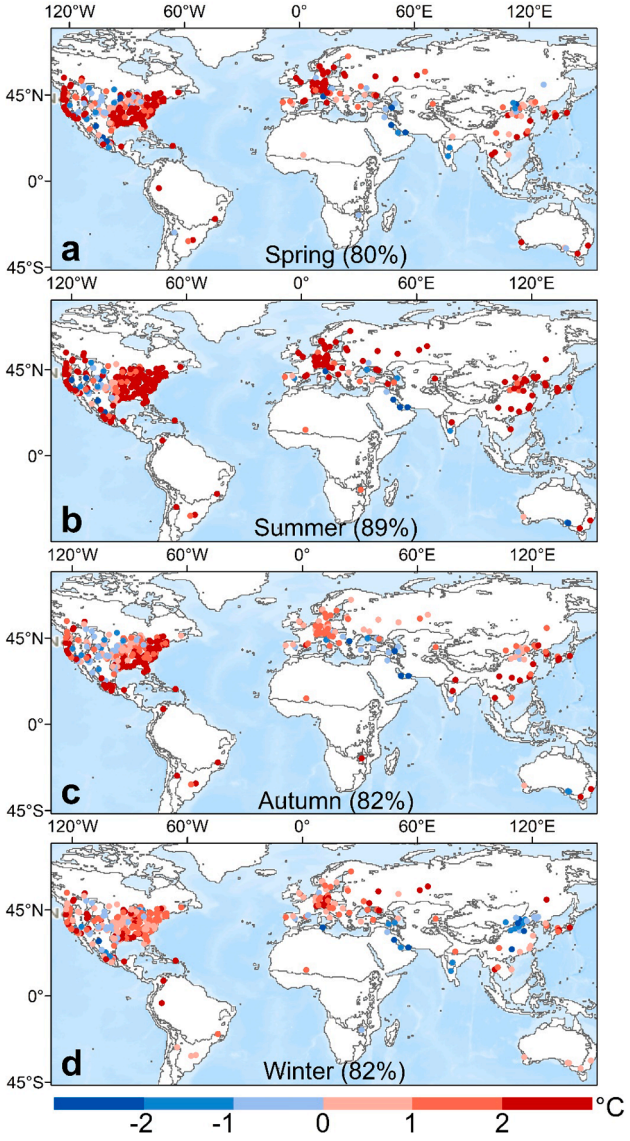

Fig. A1. Spatiotemporal patterns of SUHII during the day in different seasons. The percentages in the brackets indicate the proportion of cities with positive SUHII accounting for the total number of selected cities.

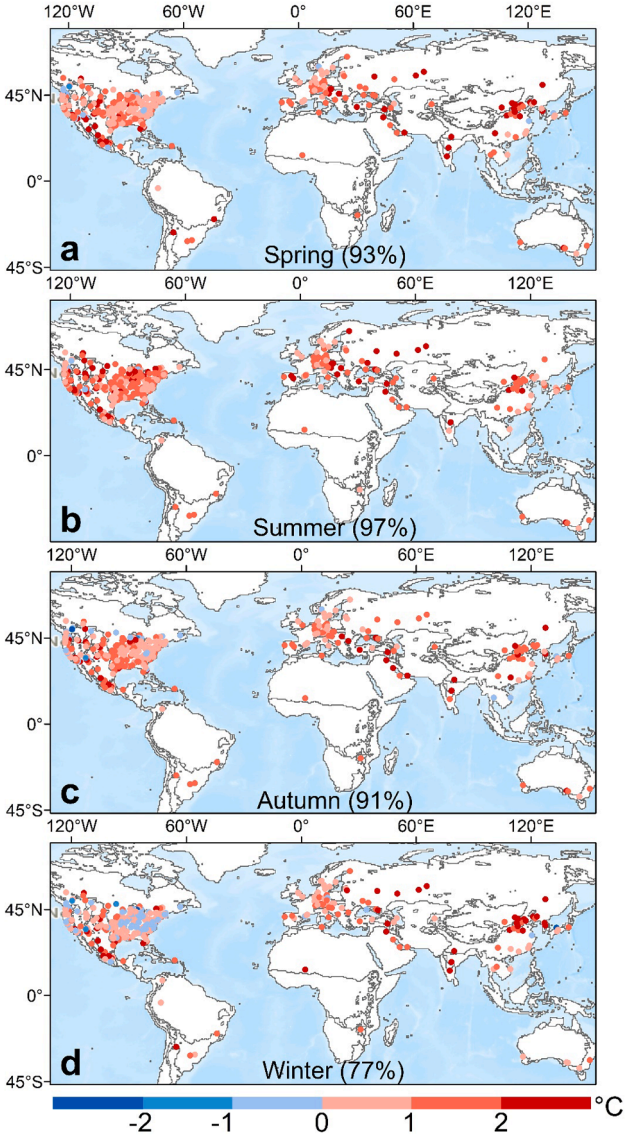

Fig. A2. Spatiotemporal patterns of SUHII during the night in different seasons.

(calculated based on all the urban and rural pixels), the annual mean difference between $SUHII_{pixel}$ (based on only pixels where urban–rural station pairs are located) and CUHII increases both during the day (2.0 °C), and night (0.4 °C).

Second, the annual mean day–night difference in SUHII (ΔSUHII) is generally positive (i.e., 0.6 ± 1.8 °C (mean ± Std)), while such a difference in CUHII (ΔCUHII) becomes negative (i.e., −0.2 ± 1.6 °C (mean ± Std)). These values suggest that urbanization increases the T_s–based DTR while decreases the T_a–based DTR. In addition, ΔSUHII was significantly higher in summer (1.5 °C) than in winter (0.2 °C), while the seasonal variation of ΔCUHII was minimal (with an amplitude of variation less than 0.15 °C). The urbanization effect on DTR also differs for cities in an arid climate, with a negative annual mean ΔCUHII (−0.2 °C) along with a negative ΔSUHII (−2.2 °C), implying that urbanization in the arid climate decreases T_a–based DTR and T_s–based DTR simultaneously. Similarly, the annual mean ΔSUHII (ΔDTR_{LST}) based on $SUHII_{pixel}$ is also greater than that based on SUHII (i.e., 1.4 °C).

Third, in terms of the controls, the impacts of vegetation abundance and ISP on SUHII and CUHII are not identical, although they are highly correlated over cities. Specifically, the urban–rural difference in ISP exerts an insignificant impact on both SUHII and CUHII during the day, yet it poses a larger impact on CUHII at night, whereas the difference in vegetation abundance exerts a greater impact on SUHII than on CUHII during the day yet the situation is reversed at night. In addition, the impacts of population size on daytime SUHII and CUHII are very close and relatively small, but their impacts on nighttime SUHII and CUHII are greater. For climatic controls, the negative impact from annual mean T_{max} is greater on SUHII than on CUHII during the day. The relationship between annual mean PREP and SUHII is positive during the day but negative at night, while for CUHII, their relationship is weakly negative regardless of day and night.

Note that the aforementioned results related to the SUHII-CUHII investigation are feasible for a large number of cities as involved in this study, although they may not be sufficiently robust for a single city owing to the use of limited urban–rural pairs of T_a measurements. Nevertheless, this study overcomes the deficiencies of previous comparisons between these two types of UHIs by conducting a simultaneous SUHI–CUHI investigation at a global scale characterized by a great variety of background climates. Note that it may be more climatologically meaningful to examine the SUHII-CUHII difference under various climates at a global scale, but decision makers should also keep a watchful eye on the climate zone where the specific city is located when

formulating appropriate heat mitigation strategies. Future investigations of SUHII and CUHII can be further promoted by using hourly *in situ* T_a data obtained from densely distributed stations as well as T_s data with relatively higher spatiotemporal resolution obtained by combining LSTs acquired from both polar and geostationary orbiters.

Declaration of Competing Interest

The authors declare that they have no known competing financial interests or personal relationships that could have appeared to influence the work reported in this paper.

Acknowledgments

This study is jointly supported by the National Key Research and Development Programs for Global Change and Adaptation (2017YFA0603604), the Jiangsu Provincial Natural Science Foundation (BK20180009), and the National Natural Science Foundation of China (42171306 and 42001270). We are also very grateful for the financial support from the National Youth Talent Support Program of China.

Appendix A. Supplementary material

Supplementary data to this article can be found online at https://doi.org/10.1016/j.isprsjprs.2021.09.003.

References

Abatzoglou, J.T., Dobrowski, S.Z., Parks, S.A., Hegewisch, K.C., 2018. TerraClimate, a high-resolution global dataset of monthly climate and climatic water balance from 1958–2015. Sci. Data 5, 1–12.
Aida, M., Yaji, M., 1979. Observations of atmospheric downward radiation in the Tokyo area. Bound.-Layer Meteor. 16, 453–465.
Anniballe, R., Bonafoni, S., Pichierri, M., 2014. Spatial and temporal trends of the surface and air heat island over Milan using MODIS data. Remote Sens. Environ. 150, 163–171.
Bonafoni, S., Anniballe, R., Pichierri, M., 2015. Comparison between surface and canopy layer urban heat island using MODIS data. In: 2015 Joint Urban Remote Sensing Event (JURSE). IEEE, pp. 1–4.
Brazel, A., Selover, N., Vose, R., Heisler, G., 2000. The tale of two climates Baltimore and Phoenix urban LTER sites. Clim. Res. 15, 123–135.
Chakraborty, T., Hsu, A., Manya, D., Sheriff, G., 2020. A spatially explicit surface urban heat island database for the United States: characterization, uncertainties, and possible applications. ISPRS-J. Photogramm. Remote Sens. 168, 74–88.
Chakraborty, T., Lee, X., 2019. A simplified urban-extent algorithm to characterize surface urban heat islands on a global scale and examine vegetation control on their spatiotemporal variability. Int. J. Appl. Earth Obs. Geoinf. 74, 269–280.
Chakraborty, T., Sarangi, C., Tripathi, S.N., 2017. Understanding diurnality and inter-seasonality of a sub-tropical urban heat island. Bound.-Layer Meteor. 163, 287–309.
Chow, W.T.L., Roth, M., 2006. Temporal dynamics of the urban heat island of Singapore. Int. J. Climatol. 26, 2243–2260.
Clinton, N., Gong, P., 2013. MODIS detected surface urban heat islands and sinks: Global locations and controls. Remote Sens. Environ. 134, 294–304.
Cui, Y., De Foy, B., 2012. Seasonal variations of the urban heat island at the surface and the near-surface and reductions due to urban vegetation in Mexico City. J. Appl. Meteorol. Climatol. 51, 855–868.
Debbage, N., Shepherd, J.M., 2015. The urban heat island effect and city contiguity. Comput. Environ. Urban Syst. 54, 181–194.
Doxsey-Whitfield, E., MacManus, K., Adamo, S.B., Pistolesi, L., Squires, J., Borkovska, O., Baptista, S.R., 2015. Taking advantage of the improved availability of census data: a first look at the gridded population of the world, version 4. Appl. Geogr. 1, 226–234.
Elmes, A., Rogan, J., Williams, C., Ratick, S., Nowak, D., Martin, D., 2017. Effects of urban tree canopy loss on land surface temperature magnitude and timing. ISPRS-J. Photogramm. Remote Sens. 128, 338–353.
Gong, P., Li, X.C., Wang, J., Bai, Y.Q., Chen, B., Hu, T.Y., Liu, X.P., Xu, B., Yang, J., Zhang, W., Zhou, Y.Y., 2020. Annual maps of global artificial impervious area (GAIA) between 1985 and 2018. Remote Sens. Environ. 236, 111510.
Good, E.J., 2016. An in situ-based analysis of the relationship between land surface "skin" and screen-level air temperatures. J. Geophys. Res.-Atmos. 121, 8801–8819.
He, B.J., 2018. Potentials of meteorological characteristics and synoptic conditions to mitigate urban heat island effects. Urban CLim. 24, 26–33.
Ho, H.C., Knudby, A., Xu, Y.M., Hodul, M., Aminipouri, M., 2016. A comparison of urban heat islands mapped using skin temperature, air temperature, and apparent temperature (Humidex), for the greater Vancouver area. Sci. Total Environ. 544, 929–938.
Homer, C., Huang, C.Q., Yang, L.M., Wylie, B., Coan, M., 2004. Development of a 2001 national land-cover database for the United States. Photogramm. Eng. Remote Sens. 70, 829–840.
Hu, Y.H., Hou, M.T., Jia, G.S., Zhao, C.L., Zhen, X.J., Xu, Y.H., 2019. Comparison of surface and canopy urban heat islands within megacities of eastern China. ISPRS-J. Photogramm. Remote Sens. 156, 160–168.
Huang, F., Zhan, W.F., Wang, Z.H., Voogt, J., Hu, L.Q., Quan, J.L., Liu, C., Zhang, N., Lai, J.M., 2020. Satellite identification of atmospheric-surface-subsurface urban heat islands under clear sky. Remote Sens. Environ. 250, 112039.
Huang, F., Zhan, W.F., Wang, Z.H., Wang, K.C., Chen, J.M., Liu, Y.X., Lai, J.M., Ju, W.M., 2017. Positive or negative? Urbanization-induced variations in diurnal skin-surface temperature range detected using satellite data. J. Geophys. Res.-Atmos. 122, 13229–13244.
Huang, X., Wang, Y., 2019. Investigating the effects of 3D urban morphology on the surface urban heat island effect in urban functional zones by using high-resolution remote sensing data: A case study of Wuhan, Central China. ISPRS-J. Photogramm. Remote Sens. 152, 119–131.
Imhoff, M.L., Zhang, P., Wolfe, R.E., Bounoua, L., 2010. Remote sensing of the urban heat island effect across biomes in the continental USA. Remote Sens. Environ. 114, 504–513.
Jin, M.S., 2012. Developing an index to measure urban heat island effect using satellite land skin temperature and land cover observations. J. Clim. 25, 6193–6201.
Jin, M.S., Dickinson, R.E., 2010. Land surface skin temperature climatology: Benefitting from the strengths of satellite observations. Environ. Res. Lett. 5, 044004.
Kottek, M., Grieser, J., Beck, C., Rudolf, B., Rubel, F., 2006. World map of the Köppen-Geiger climate classification updated. Meteorol. Z. 15, 259–263.
Lai, J.M., Zhan, W.F., Huang, F., Voogt, J., Bechtel, B., Allen, M., Peng, S.S., Hong, F.L., Liu, Y.X., Du, P.J., 2018. Identification of typical diurnal patterns for clear-sky climatology of surface urban heat islands. Remote Sens. Environ. 217, 203–220.
Lai, J.M., Zhan, W.F., Voogt, J., Quan, J.L., Huang, F., Zhou, J., Bechtel, B., Hu, L.Q., Wang, K.C., Cao, C., 2021. Meteorological controls on daily variations of nighttime surface urban heat islands. Remote Sens. Environ. 253, 112198.
Li, D., Liao, W.L., Rigden, A.J., Liu, X.P., Wang, D.G., Malyshev, S., Shevliakova, E., 2019. Urban heat island: Aerodynamics or imperviousness? Sci. Adv. 5, eaau4299.
Li, J.F., Zhan, W.F., Hong, F.L., Lai, J.M., Dong, P., Liu, Z.H., Wang, C.G., Huang, F., Li, L., Wang, C.L., Fu, Y.C., Miao, S.Q., 2021. Similarities and disparities in urban local heat islands responsive to regular-, stable-, and counter-urbanization: A case study of Guangzhou. China. Build. Environ. 199, 107935.
Li, L., Huang, X., Li, J.Y., Wen, D.W., 2017. Quantifying the spatiotemporal trends of canopy layer heat island (CLHI) and its driving factors over Wuhan, China with satellite remote sensing. Remote Sens. 9, 536.
Li, L., Zha, Y., 2019. Satellite-based spatiotemporal trends of canopy urban heat islands and associated drivers in China's 32 major cities. Remote Sens. 11, 102.
Li, L., Zha, Y., Wang, R., 2020a. Relationship of surface urban heat island with air temperature and precipitation in global large cities. Ecol. Indic. 117, 106683.
Li, L., Zha, Y., Zhang, J.H., 2020b. Spatially non-stationary effect of underlying driving factors on surface urban heat islands in global major cities. Int. J. Appl. Earth Obs. Geoinf. 90, 102131.
Li, X.C., Gong, P., Zhou, Y.Y., Wang, J., Bai, Y.Q., Chen, B., Hu, T.Y., Xiao, Y.X., Xu, B., Yang, J., 2020c. Mapping global urban boundaries from the global artificial impervious area (GAIA) data. Environ. Res. Lett. 15, 094044.
Li, Z.L., Tang, B.H., Wu, H., Ren, H.Z., Yan, G.J., Wan, Z.M., Trigo, I.F., Sobrino, J.A., 2013. Satellite-derived land surface temperature: Current status and perspectives. Remote Sens. Environ. 131, 14–37.
Manoli, G., Fatichi, S., Bou-Zeid, E., Katul, G.G., 2020a. Seasonal hysteresis of surface urban heat islands. Proc. Natl. Acad. Sci. 117, 7082–7089.
Manoli, G., Fatichi, S., Schläpfer, M., Yu, K., Crowther, T.W., Meili, N., Burlando, P., Katul, G.G., Bou-Zeid, E., 2020b. Reply to Martilli et al. (2020): Summer average urban-rural surface temperature differences do not indicate the need for urban heat reduction. OSF Preprints. https://doi.org/10.31219/osf.io/mwpna.
Manoli, G., Fatichi, S., Schläpfer, M., Yu, K., Crowther, T.W., Meili, N., Burlando, P., Katul, G.G., Bou-Zeid, E., 2019. Magnitude of urban heat islands largely explained by climate and population. Nature 573, 55–60.
Martilli, A., Krayenhoff, E.S., Nazarian, N., 2020a. Is the urban heat island intensity relevant for heat mitigation studies? Urban CLim. 31, 100541.
Martilli, A., Roth, M., Chow, W.T., Demuzere, M., Lipson, M., Krayenhoff, E.S., Sailor, D., Nazarian, N., Voogt, J., Wouters, H., 2020b. Summer average urban-rural surface temperature differences do not indicate the need for urban heat reduction. OSF Preprints. https://doi.org/10.31219/osf.io/8gnbf.
Miles, V., Esau, I., 2020. Surface urban heat islands in 57 cities across different climates in northern Fennoscandia. Urban CLim. 31, 100575.
Mirzaee, S., Özgun, O., Ruth, M., Binita, K., 2018. Neighborhood-scale sky view factor variations with building density and height: A simulation approach and case study of Boston. Urban CLim. 26, 95–108.
Morris, C., Simmonds, I., Plummer, N., 2001. Quantification of the influences of wind and cloud on the nocturnal urban heat island of a large city. J. Appl. Meteorol. Climatol. 40, 169–182.
OECD, 2021. Urban population by city size (indicator). https://doi.org/10.1787/b4332f92-en (accessed on 24 March 2021).
Oke, T.R., 1973. City size and the urban heat island. Atmos. Environ. 7, 769–779.
Oke, T.R., 1982. The energetic basis of the urban heat island. Q. J. R. Meteorol. Soc. 108, 1–24.
Oke, T.R., 2004. Initial guidance to obtain representative meteorological observations at urban sites. IOM Report No.81, WMO/TD. No.1250, World Meteorological Organization, Geneva.

Oke, T.R., Mills, G., Christen, A., Voogt, J.A., 2017. Urban climates. Cambridge University Press.
Oleson, K.W., Monaghan, A., Wilhelmi, O., Barlage, M., Brunsell, N., Feddema, J., Hu, L. M., Steinhoff, D., 2015. Interactions between urbanization, heat stress, and climate change. Clim. Change 129, 525–541.
Paschalis, A., Chakraborty, T., Fatichi, S., Meili, N., Manoli, G., 2021. Urban forests as main regulator of the evaporative cooling effect in cities. AGU Advances. 2, e2020AV000303.
Peng, S.S., Piao, S.L., Ciais, P., Friedlingstein, P., Ottle, C., Breon, F.M., Nan, H.J., Zhou, L.M., Myneni, R.B., 2012. Surface urban heat island across 419 global big cities. Environ. Sci. Technol. 46, 696–703.
Pugachev, V.S., 2014. Probability theory and mathematical statistics for engineers. Elsevier.
Ridd, M.K., 1995. Exploring a VIS (vegetation-impervious surface-soil) model for urban ecosystem analysis through remote sensing: comparative anatomy for cities. Int. J. Remote Sens. 16, 2165–2185.
Rohde, R., Muller, R., Jacobsen, R., Perlmutter, S., Rosenfeld, A., Wurtele, J., Curry, J., Wickham, C., Mosher, S., 2013. Berkeley earth temperature averaging process. Geoinform. Geostatistics: Overview 1. https://doi.org/10.4172/2327-4581.1000103.
Santamouris, M., 2020. Recent progress on urban overheating and heat island research. Integrated assessment of the energy, environmental, vulnerability and health impact. Synergies with the global climate change. Energy Build. 207, 109482.
Schwarz, N., Schlink, U., Franck, U., Großmann, K., 2012. Relationship of land surface and air temperatures and its implications for quantifying urban heat island indicators—An application for the city of Leipzig (Germany). Ecol. Indic. 18, 693–704.
Sheng, L., Tang, X.L., You, H.Y., Gu, Q., Hu, H., 2017. Comparison of the urban heat island intensity quantified by using air temperature and Landsat land surface temperature in Hangzhou. China. Ecol. Indic. 72, 738–746.
Song, X.P., Sexton, J.O., Huang, C.Q., Channan, S., Townshend, J.R., 2016. Characterizing the magnitude, timing and duration of urban growth from time series of Landsat-based estimates of impervious cover. Remote Sens. Environ. 175, 1–13.
Stewart, I.D., 2011. A systematic review and scientific critique of methodology in modern urban heat island literature. Int. J. Climatol. 31, 200–217.
Stewart, I.D., 2019. Why should urban heat island researchers study history? Urban CLim. 30, 100484.
Stewart, I.D., Oke, T.R., 2012. Local climate zones for urban temperature studies. Bull. Amer. Meteorol. Soc. 93, 1879–1900.
Sun, H., Chen, Y.H., Zhan, W.F., 2015. Comparing surface- and canopy-layer urban heat islands over Beijing using MODIS data. Int. J. Remote Sens. 36, 5448–5465.
Sun, L., Chen, Z.X., Gao, F., Anderson, M., Song, L.S., Wang, L.M., Hu, B., Yang, Y., 2017. Reconstructing daily clear-sky land surface temperature for cloudy regions from MODIS data. Comput. Geosci. 105, 10–20.
Sun, T., Sun, R.H., Chen, L.D., 2020. The trend inconsistency between land surface temperature and near surface air temperature in assessing urban heat island effects. Remote Sens. 12, 1271.
Sun, Y.M., Augenbroe, G., 2014. Urban heat island effect on energy application studies of office buildings. Energy Build. 77, 171–179.
Tam, B.Y., Gough, W.A., Mohsin, T., 2015. The impact of urbanization and the urban heat island effect on day to day temperature variation. Urban CLim. 12, 1–10.
Tan, J.G., Zheng, Y.F., Tang, X., Guo, C.Y., Li, L.P., Song, G.X., Zhen, X.R., Yuan, D., Kalkstein, A.J., Li, F.R., 2010. The urban heat island and its impact on heat waves and human health in Shanghai. Int. J. Biometeorol. 54, 75–84.
Tysa, S.K., Ren, G.Y., Qin, Y., Zhang, P.F., Ren, Y.Y., Jia, W.Q., Wen, K.M., 2019. Urbanization effect in regional temperature series based on a remote sensing classification scheme of stations. J. Geophys. Res.-Atmos. 124, 10646–10661.
Varquez, A.C.G., Kanda, M., 2018. Global urban climatology: a meta-analysis of air temperature trends (1960-2009). NPJ Clim. Atmos. Sci. 1, 32.
Venter, Z.S., Chakraborty, T., Lee, X.H., 2021. Crowdsourced air temperatures contrast satellite measures of the urban heat island and its mechanisms. Sci. Adv. 7, eabb9569.
Wan, Z.M., Dozier, J., 1996. A generalized split-window algorithm for retrieving land-surface temperature from space. Int. J. Remote Sens. 34, 892–905.
Wang, K.C., Jiang, S.J., Wang, J.K., Zhou, C.L., Wang, X.Y., Lee, X.H., 2017. Comparing the diurnal and seasonal variabilities of atmospheric and surface urban heat islands based on the Beijing urban meteorological network. J. Geophys. Res.-Atmos. 122, 2131–2154.
Wang, K.C., Wang, J.K., Wang, P.C., Sparrow, M., Yang, J., Chen, H.B., 2007. Influences of urbanization on surface characteristics as derived from the Moderate-Resolution Imaging Spectroradiometer: A case study for the Beijing metropolitan area. J. Geophys. Res.-Atmos. 112.
Wang, W., Yao, X.F., Shu, J., 2020. Air advection induced differences between canopy and surface heat islands. Sci. Total Environ. 725, 138120.
Wang, W.C., Zeng, Z., Karl, T.R., 1990. Urban heat islands in China. Geophys. Res. Lett. 17, 2377–2380.
Weng, Q.H., 2009. Thermal infrared remote sensing for urban climate and environmental studies: Methods, applications, and trends. ISPRS-J. Photogramm. Remote Sens. 64, 335–344.
Wohlfahrt, G., Tomelleri, E., Hammerle, A., 2019. The urban imprint on plant phenology. Nat. Ecol. Evol. 3, 1668–1674.
Wong, M.S., Nichol, J., Ng, E., 2011. A study of the "wall effect" caused by proliferation of high-rise buildings using GIS techniques. Landsc. Urban Plan. 102, 245–253.
Yang, C.B., Yan, F.Q., Zhang, S.W., 2020. Comparison of land surface and air temperatures for quantifying summer and winter urban heat island in a snow climate city. J. Environ. Manage. 265, 110563.
Yang, J., Bou-Zeid, E., 2018. Should cities embrace their heat islands as shields from extreme cold? J. Appl. Meteorol. Climatol. 57, 1309–1320.
Zhang, F., Cai, X.M., Thornes, J.E., 2014a. Birmingham's air and surface urban heat islands associated with Lamb weather types and cloudless anticyclonic conditions. Prog. Phys. Geogr. 38, 431–447.
Zhang, P., Bounoua, L., Imhoff, M.L., Wolfe, R.E., Thome, K., 2014b. Comparison of MODIS land surface temperature and air temperature over the continental USA meteorological stations. Can. J. Remote Sens. 40, 110–122.
Zhao, L., Lee, X.H., Smith, R.B., Oleson, K., 2014. Strong contributions of local background climate to urban heat islands. Nature 511, 216–219.
Zhao, L., Oppenheimer, M., Zhu, Q., Baldwin, J.W., Ebi, K.L., Bou-Zeid, E., Guan, K.Y., Liu, X., 2018. Interactions between urban heat islands and heat waves. Environ. Res. Lett. 13, 034003.